Molecular Cell
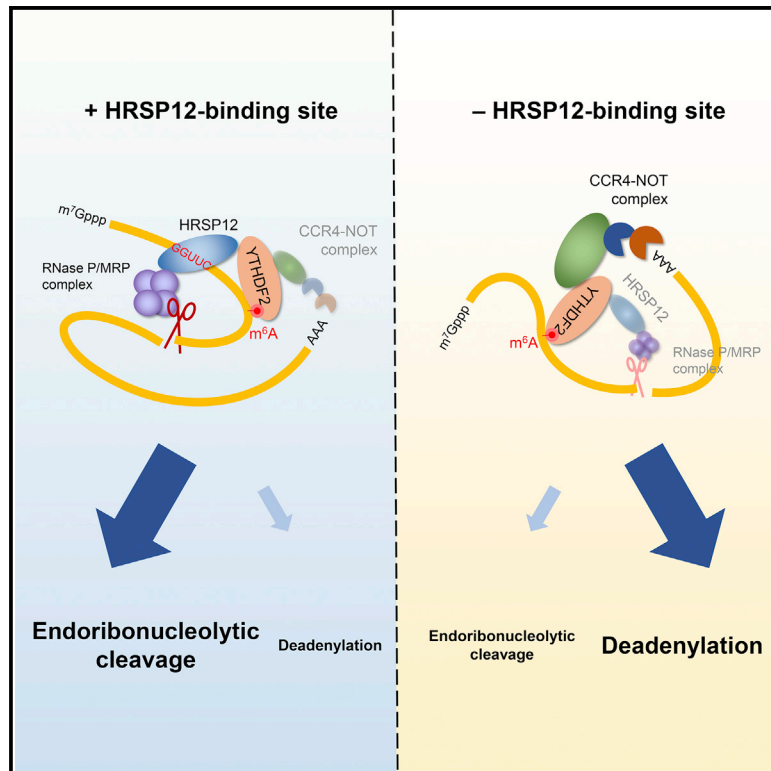
Endoribonucleolytic Cleavage of m^{6}A-Containing RNAs by RNase P/MRP Complex

Graphical Abstract

Authors

Ok Hyun Park, Hongseok Ha, Yujin Lee, Sung Ho Boo, Do Hoon Kwon, Hyun Kyu Song, Yoon Ki Kim

Correspondence

yk-kim@korea.ac.kr

In Brief

m^{6}A-containing RNAs are known to be recognized and destabilized by YTHDF2. However, the underlying molecular mechanisms remain unclear. Park et al. show that m^{6}A-containing linear and circular RNAs are endoribonucleolytically cleaved by a YTHDF2-HRSP12-RNase P/MRP axis.

Highlights

- m^{6}A-containing RNAs are degraded by an endoribonucleolytic cleavage pathway

- A YTHDF2-HRSP12-RNase P/MRP axis contributes to m^{6}A-mediated RNA decay

- An interaction between YTHDF2 and RNase P/MRP is bridged by HRSP12

- m^{6}A-containing circular RNAs are degraded by the YTHDF2-HRSP12-RNase P/MRP pathway

CellPress

Article

Endoribonucleolytic Cleavage of m^{6}A-Containing RNAs by RNase P/MRP Complex

Ok Hyun Park,[1,2,3] Hongseok Ha,[1,2,3] Yujin Lee,[1,2] Sung Ho Boo,[1,2] Do Hoon Kwon,[2] Hyun Kyu Song,[2] and Yoon Ki Kim[1,2,4,*]
[1]Creative Research Initiatives Center for Molecular Biology of Translation, Korea University, Seoul 02841, Republic of Korea
[2]Division of Life Sciences, Korea University, Seoul 02841, Republic of Korea
[3]These authors contributed equally
[4]Lead Contact
*Correspondence: yk-kim@korea.ac.kr
https://doi.org/10.1016/j.molcel.2019.02.034

SUMMARY

N^6-methyladenosine (m^{6}A) is the most abundant internal modification in RNAs and plays regulatory roles in a variety of biological and physiological processes. Despite its important roles, the molecular mechanism underlying m^{6}A-mediated gene regulation is poorly understood. Here, we show that m^{6}A-containing RNAs are subject to endoribonucleolytic cleavage via YTHDF2 (m^{6}A reader protein), HRSP12 (adaptor protein), and RNase P/MRP (endoribonucleases). We demonstrate that HRSP12 functions as an adaptor to bridge YTHDF2 and RNase P/MRP, eliciting rapid degradation of YTHDF2-bound RNAs. Transcriptome-wide analyses show that m^{6}A RNAs that are preferentially targeted for endoribonucleolytic cleavage have an HRSP12-binding site and a RNase P/MRP-directed cleavage site upstream and downstream of the YTHDF2-binding site, respectively. We also find that a subset of m^{6}A-containing circular RNAs associates with YTHDF2 in an HRSP12-dependent manner and is selectively downregulated by RNase P/MRP. Thus, our data expand the known functions of RNase P/MRP to endoribonucleolytic cleavage of m^{6}A RNAs.

INTRODUCTION

Considerable recent studies revealed the importance of post-transcriptional RNA modifications in shaping an epitranscriptomic landscape of gene expression (Meyer and Jaffrey, 2017; Yang et al., 2018). To date, more than 100 distinct types of RNA modifications have been characterized. Among them, methylation of the 6-amino group of adenosine to generate N^6-methyladenosine (m^{6}A) is the most abundant internal modification of RNAs (Dominissini et al., 2012; Meyer et al., 2012). m^{6}A modification is dynamically and reversibly regulated by three classes of proteins (Meyer and Jaffrey, 2017; Roundtree et al., 2017a; Yang et al., 2018). In the case of mammalian cells, generation of m^{6}A is catalyzed by a multiprotein methyltransferase

complex containing METTL3, METTL14, and WTAP (Meyer and Jaffrey, 2017; Yang et al., 2018). m^{6}As in RNAs are selectively recognized by m^{6}A-specific binding proteins, such as YT521-B homology (YTH)-domain-containing proteins, hnRNPs, and eIF3 (Alarcón et al., 2015; Dominissini et al., 2012; Meyer et al., 2015; Wang et al., 2014). Demethylases such as FTO and ALKBH5 are involved in the removal of m^{6}A (Jia et al., 2011; Zheng et al., 2013).

Recent research revealed that m^{6}A in RNAs exerts regulatory functions in a broad spectrum of biological and physiological processes (Fu et al., 2014; Meyer and Jaffrey, 2017; Roundtree et al., 2017a; Yang et al., 2018). At the molecular level, m^{6}A is known to affect mRNA stability, mRNA translation, microRNA biogenesis, and splicing, most of which are mediated by specific m^{6}A-binding proteins. For instance, YTHDF2, one of the YTH-domain-containing proteins, destabilizes m^{6}A-containing RNAs (Du et al., 2016; Wang et al., 2014). YTHDF1 and YTHDF3 promote translation of m^{6}A mRNAs (Li et al., 2017; Wang et al., 2015). In addition, YTHDC1 is known to regulate pre-mRNA splicing and nuclear export of m^{6}A mRNAs (Roundtree et al., 2017b; Xiao et al., 2016).

Eukaryotic RNase P and its close relative RNase MRP are essential ribonucleoprotein complexes that function as endoribonucleases (Jarrous, 2017). Mammalian RNase P and RNase MRP contain common protein components (in the order of their molecular weight: POP1, RPP38, POP5, RPP25, RPP20, RPP30, and RPP40) and their unique protein components with their unique noncoding RNA components, *RPPH1* and *RMRP* RNAs, respectively. Originally, RNase P and RNase MRP were identified to be the endoribonucleases responsible for the maturation of tRNA and mitochondrial RNA processing of replication primers, respectively. Nonetheless, it was later shown that eukaryotic RNase P and RNase MRP are involved in the cleavage of a wide range of RNA substrates, such as rRNAs, long noncoding RNAs, and mRNAs (Coughlin et al., 2008; Jarrous, 2017; Maida et al., 2009; Wilusz et al., 2008).

Despite the biological importance of the aforementioned m^{6}A modification, the molecular mechanisms underlying m^{6}A-mediated gene regulation are poorly understood. In this study, we report that m^{6}A RNAs are endoribonucleolytically cleaved by a YTHDF2-HRSP12-RNase P/MRP axis. These findings shed light on the molecular mechanisms of multilayered gene regulation mediated by m^{6}A modification in RNA.
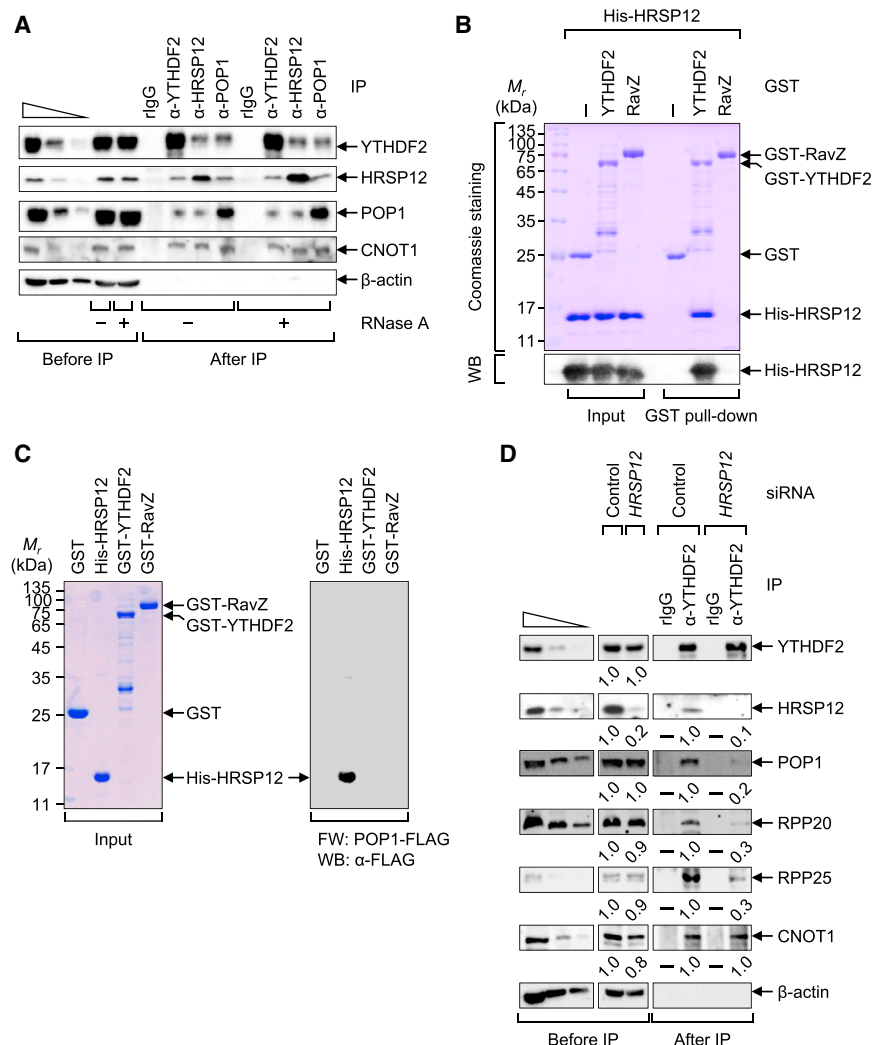
Figure 1. HRSP12 Serves as an Adaptor Protein for the Association of YTHDF2 and RNase P/MRP

(A) Immunoprecipitation (IP) of endogenous YTHDF2, HRSP12, or POP1. IPs were carried out using either the indicated antibody or rabbit IgG (rIgG) as a control and the extracts of HEK293T cells either treated or not treated with RNase A. To demonstrate that the western blotting (WB) was semiquantitative, the total-cell extracts serially diluted 3-fold were loaded in the three leftmost lanes.

(B) *In vitro* GST pull-down assays. Purified recombinant His-HRSP12 was mixed with purified recombinant GST, GST-YTHDF2, or GST-RavZ (as a negative control). After GST pull-down, the purified proteins were subjected to either Coomassie blue staining (upper) or WB (lower) with an anti (α)-His antibody. Note that the arrow for GST-YTHDF2 indicates C-terminally deleted form during recombinant protein purification.

(C) Far-western blotting (FW) of purified recombinant proteins. Left: Coomassie blue staining of purified recombinant proteins showing the integrity and relative abundance levels of the input. Right: FW with immunopurified POP1-FLAG as a probe.

(D) IP of YTHDF2 using the RNase A-treated extracts of HEK293T cells depleted of HRSP12. As performed in (A), except that the cells were either not depleted or depleted of HRSP12.

All data represent at least two independently studied biological replicates (n = 2).

RESULTS

HRSP12 Links YTHDF2 and RNase P/MRP

An interaction between Pho92 (a yeast homolog of human YTHDF2) and Mmf1 (a yeast homolog of human heat-responsive protein 12 [HRSP12]) was experimentally identified by tandem affinity purification (Krogan et al., 2006). In addition, a large-scale *de novo* prediction of physical protein–protein association using a combined random forests and Bayesian learning strategy predicted an interaction between HRSP12 and POP1, a component of RNase P/MRP (Elefsinioti et al., 2011). In this study, we set out to assess the predicted interactions by *in vivo* and *in vitro* experimental approaches.

Immunoprecipitation (IP) experiments revealed that YTHDF2, HRSP12, and POP1 were complexed with one another in an RNase A-resistant manner (Figures 1A and S1A). The previously known YTHDF2-interacting protein CNOT1 (a component of the CCR4-NOT deadenylase complex [Du et al., 2016]) was also selectively enriched in the IPs. Of note, YTHDF1 and YTHDF3, two paralogs of YTHDF2, were only marginally enriched in the immunoprecipitates of HRSP12 (Figure S1B), pointing to preferential association between YTHDF2 and HRSP12. *In vitro* GST pull-down experiments showed that purified recombinant His-HRSP12 was selectively enriched in the pull-down of GST-YTHDF2, but not GST or GST-RavZ (a negative control protein; Figures 1B and S1C), indicating a direct interaction between YTHDF2 and HRSP12. In addition, far-western blotting involving purified recombinant proteins and either immunopurified FLAG-GFP (Figures S1D and S1E) or POP1-FLAG (Figures 1C and S1D) as a probe revealed a direct interaction between HRSP12 and POP1. Collectively, our data showed that human HRSP12 directly interacts with YTHDF2 and RNase P/MRP. Considering that most of HRSP12 and YTHDF2 were enriched in the cytoplasmic fraction and that POP1 was distributed throughout the cell (Figure S1F), it is likely that the complex formation largely occurs in the cytoplasm.

In the above-mentioned far-western blotting, the immunopurified POP1-FLAG probe reacted only with His-HRSP12 (not GST-YTHDF2), suggesting a lack of a direct interaction between YTHDF2 and RNase P/MRP. Given that YTHDF2, HRSP12, and POP1 form a complex (Figure 1A), these observations pointed to a possible role of HRSP12 in bridging YTHDF2 and RNase P/MRP. In support of this possibility, when HRSP12 was downregulated 5-fold by treatment of the cells with small interfering RNAs (siRNAs), 3- to 5-fold smaller amounts of components of RNase P/MRP (POP1, RPP20, and RPP25) coimmunoprecipitated (coIPed) in the IP of YTHDF2 (Figure 1D).
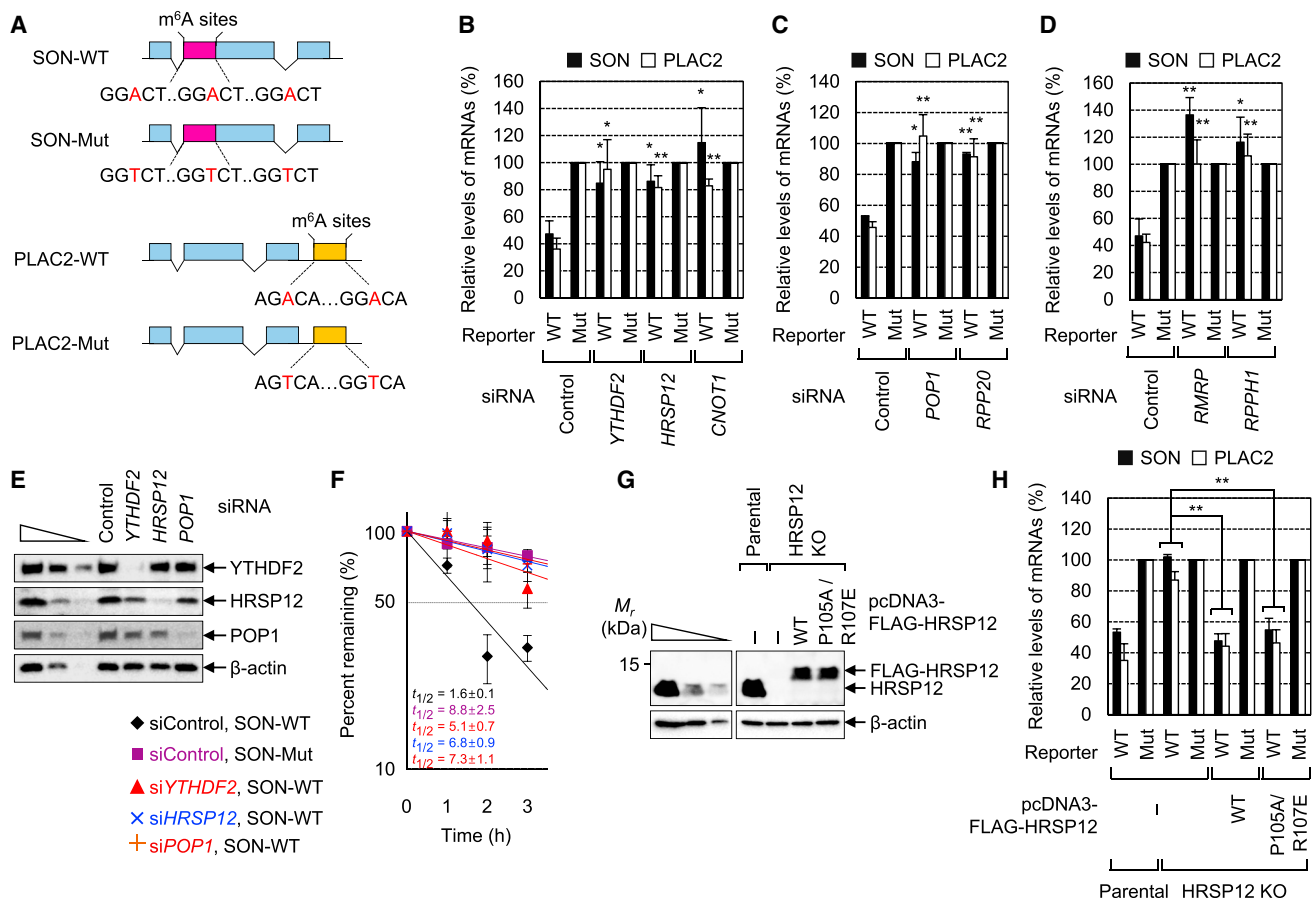
Figure 2. Downregulation of YTHDF2, HRSP12, or an RNase P/MRP Component Inhibits m⁶A-Mediated mRNA Decay

(A) Schematic representation of m⁶A reporter mRNAs. The m⁶A target sites are highlighted in red.

(B–D) Effects of downregulation of the indicated protein or RNA on the abundance of m⁶A reporter mRNA. HeLa cells were transiently transfected with the indicated siRNA. One day later, the cells were cotransfected with one of the reporter plasmids and with phCMV-MUP as a reference plasmid. Two days later, total-RNA samples were prepared and analyzed by quantitative real-time RT-PCR (qRT-PCR). The levels of m⁶A reporter mRNAs were normalized to those of *MUP* mRNA. The normalized levels of m⁶A Mut reporter mRNAs were arbitrarily set to 100%. n = 3 for (B) and (C); n = 5 for (D); *p < 0.05; **p < 0.01.

(E and F) The influence of downregulation of the indicated protein on the half-life of m⁶A reporter mRNA. As performed in (B)–(D), except that the cells were treated with 5,6-dichloro-1-β-D-ribofuranosylbenzimidazole (DRB, a potent transcription inhibitor) before cell harvesting.

(E) WB showing the specific downregulation.

(F) mRNA half-life plotted as a function of time. Total-RNA samples were prepared at the indicated time points. The levels of m⁶A reporter mRNAs were normalized to those of *MUP* mRNA. The normalized levels at 0 h were arbitrarily set to 100%. The y axis represents the level of mRNA remaining (percentage) on the logarithmic scale.

(G and H) Complementation experiments using either parental or HRSP12-KO HAP1 cells and transiently expressed FLAG-HRSP12 or its variant. Parental or HRSP12-KO HAP1 cells were transiently cotransfected with one of the m⁶A reporter plasmids, phCMV-MUP, and a plasmid expressing FLAG-HRSP12 or its variant.

(G) WB proving a specific KO of HRSP12 and comparable expression of FLAG-HRSP12 and its variant.

(H) The efficiency of m⁶A-mediated mRNA decay. n = 3; **p < 0.01.

Two-tailed, equal-sample-variance Student's t test was conducted to calculate the p values.

Notably, the known interaction between YTHDF2 and CNOT1 was affected only marginally. Therefore, our observations indicated that HRSP12 is a molecular linker bridging YTHDF2 and RNase P/MRP.

Downregulation of HRSP12 or RNase P/MRP Components Abrogates m⁶A-Mediated mRNA Decay

An m⁶A mRNA is destabilized under the influence of YTHDF2 (Wang et al., 2014). On the basis of our observations regarding for-

mation of a complex of YTHDF2, HRSP12, and RNase P/MRP (Figure 1), we investigated a possible function of HRSP12 and RNase P/MRP in m⁶A-mediated mRNA decay. To this end, the two different previously established m⁶A β-globin reporter systems (Du et al., 2016) were employed (Figure 2A). SON-WT and SON-Mut reporter mRNAs contained β-globin genomic sequences harboring three m⁶A target sites derived from the wild-type (WT) *SON* gene (SON-WT) and the mutated version (Mut) of the corresponding sequences (SON-Mut) within the

open reading frame, respectively. PLAC2-WT and PLAC2-Mut mRNAs contained two m⁶A target sites derived from the *PLAC2* gene (PLAC2-WT) and the mutated version of the corresponding sequences (PLAC2-Mut), respectively, in the 3′ UTR. The inserted m⁶A target sites derived from genes SON and PLAC2 were confirmed to be m⁶A methylated and bound to YTHDF2 in our present (Figure S2A) and previous studies (Du et al., 2016; Wang et al., 2014).

Both SON-WT and PLAC2-WT mRNAs showed ∼40%–50% lower abundance relative to their corresponding Mut mRNAs (Figures 2B–2D). The relative decrease in abundance was reversed when METTL3 or METTL14 was downregulated (Figures S2B and S2C), validating specific m⁶A-mediated reporter mRNA decay. Of note, downregulation of endogenous YTHDF2, HRSP12, or a protein component (POP1 or RPP20) or an RNA component (*RMRP* or *RPPH1*) of RNase P/MRP increased the relative abundance (Figures 2B–2D and S2D–S2F) and half-life (Figures 2E and 2F) of WT reporter mRNAs, indicating that HRSP12 and RNase P/MRP function in m⁶A-mediated mRNA decay. Although we cannot completely rule out the possible indirect effect caused by inefficient processing of rRNAs or tRNAs by downregulation of a component of RNase P/MRP, all the data indicate that HRSP12 and RNase P/MRP function in m⁶A-mediated mRNA decay. In addition, consistent with a report showing that YTHDF2 triggers m⁶A-mediated RNA decay with the help of the CCR4-NOT deadenylase complex (Du et al., 2016), downregulation of CNOT1 also increased the relative levels of WT mRNAs (Figure 2B).

To further dissect the role of HRSP12, we generated HRSP12 knockout (KO) HAP1 cells: near-haploid human cell lines originating from a patient with chronic myeloid leukemia (Blomen et al., 2015; Carette et al., 2011). Whereas both SON-WT and PLAC2-WT mRNAs decreased in abundance in the parental HAP1 cells, their levels were comparable to the levels of Mut mRNAs in HRSP12-KO HAP1 cells (Figures 2G and 2H), supporting our conclusion about participation of HRSP12 in m⁶A-mediated mRNA decay.

m⁶A-Mediated mRNA Decay Is Mechanistically Different from Glucocorticoid Receptor (GR)-Mediated mRNA Decay (GMD)

Previous reports showed that HRSP12 participates in GMD, which is induced by a glucocorticoid (GC), a specific GR ligand (Cho et al., 2015; Park et al., 2016). In GMD, a ligand-free GR directly binds to a subset of mRNAs. In the presence of GC, the mRNA-bound GR associates with GC, providing a favorable platform for the loading of HRSP12, triggering effective GMD of GR-bound mRNAs. Therefore, given that HRSP12 is a GMD component, it is possible that m⁶A-mediated mRNA decay is affected by GMD or vice versa.

Although treatment with dexamethasone (Dex), which is a synthetic derivative of a GC, did not affect m⁶A-mediated mRNA decay of both *SON* and *PLAC2* reporter mRNAs (Figure S2G), the level of an endogenous GMD substrate, *CCL2* mRNA, drastically decreased after Dex treatment (Figure S2H). Furthermore, downregulation of POP1 did not affect GMD (Figures S2I and S2J). As expected, both m⁶A-mediated mRNA decay and GMD were inhibited by HRSP12 downregulation (Figures 2B and

S2J). In addition, complementation of HRSP12 through expression of exogenous FLAG-HRSP12-WT in HRSP12-KO HAP1 cells restored the efficiency of both m⁶A-mediated mRNA decay (Figures 2G and 2H) and GMD (Figures S2K and S2L). Of note, although exogenously expressed FLAG-HRSP12-P105A/R107E successfully restored m⁶A-mediated mRNA decay (Figures 2G and 2H), it failed to restore the functionality of GMD (Figures S2K and S2L). It is known that the HRSP12-P105A/R107E variant cannot form a trimeric structure and fails to maintain the structural integrity of a functionally active GMD complex (Park et al., 2016). These data suggest that GMD, but not m⁶A-mediated mRNA decay, requires the trimerization motif of HRSP12. Collectively, our data indicated that m⁶A-mediated mRNA decay is mechanistically distinct from GMD.

N-Terminal 100 Amino Acid (aa) Residues of YTHDF2 Are Sufficient for Eliciting RNA Decay via HRSP12

To delineate the minimal functional region of YTHDF2 for m⁶A-mediated RNA decay involving HRSP12, YTHDF2 was artificially tethered to the 3′ UTR of a reporter mRNA using the bacteriophage MS2 coat protein (MS2) and its binding site (MS2bs; Figure 3A). In parental HAP1 cells, artificially tethered MS2-HA-YTHDF2 and MS2-HA-SMG5, but not MS2-HA-GFP, elicited rapid degradation of reporter mRNA (Figures 3B and S3A). SMG5, a specific cellular factor for nonsense-mediated mRNA decay, is known to elicit rapid mRNA degradation when it is tethered to the 3′ UTR of a reporter mRNA (Cho et al., 2013). It is noteworthy that the observed rapid mRNA degradation by the tethered YTHDF2, but not by the tethered SMG5, was drastically inhibited in HRSP12-KO HAP1 cells, suggesting that YTHDF2-mediated RNA degradation specifically depends on HRSP12.

We next generated two deletion variants of YTHDF2 (Figure 3A): YTHDF-N (lacking a YTH domain in a C-terminal region) and YTHDF-C (lacking a P/Q/N-rich low-complexity region without a clear domain in the N-terminal part). The IP results showed that HRSP12, POP1, RPP25, and CNOT1 coIPed with the full-length YTHDF2 and YTHDF2-N, but not with YTHDF2-C (Figure 3C). In agreement with the IP results, tethered YTHDF2 and YTHDF2-N, but not YTHDF2-C, elicited rapid mRNA degradation in an HRSP12-dependent manner (Figures 3D and S3B).

The N-terminal region of YTHDF2 was further subdivided into four segments: aa 1–100, aa 101–200, NΔ101–200, and aa 201–383 (Figure 3A). We carried out GST pull-down experiments using the extracts of cells expressing GST-HRSP12 and one of the deletion variants of YTHDF2 (Figure 3E). Variants YTHDF2-N, 1–100, and NΔ101–200 were significantly enriched in the pull-down of GST-HRSP12. Variant 201–383 was only weakly enriched in the pull-down. In contrast, variant 101–200, which is known to directly interact with CNOT1 (Du et al., 2016), was undetectable in the pull-down. In line with the GST pull-down results, artificial tethering of variants N, 1–100, or NΔ101–200 elicited rapid mRNA degradation in an HRSP12-dependent manner (Figures 3F and S3C). In addition, variant 201–383, which manifested a weak interaction with HRSP12, caused slight mRNA downregulation without a significant dependence on HRSP12. Of note, tethered variant 101–200 elicited rapid mRNA degradation in an HRSP12-independent manner, probably via the CNOT1 interaction, suggesting that
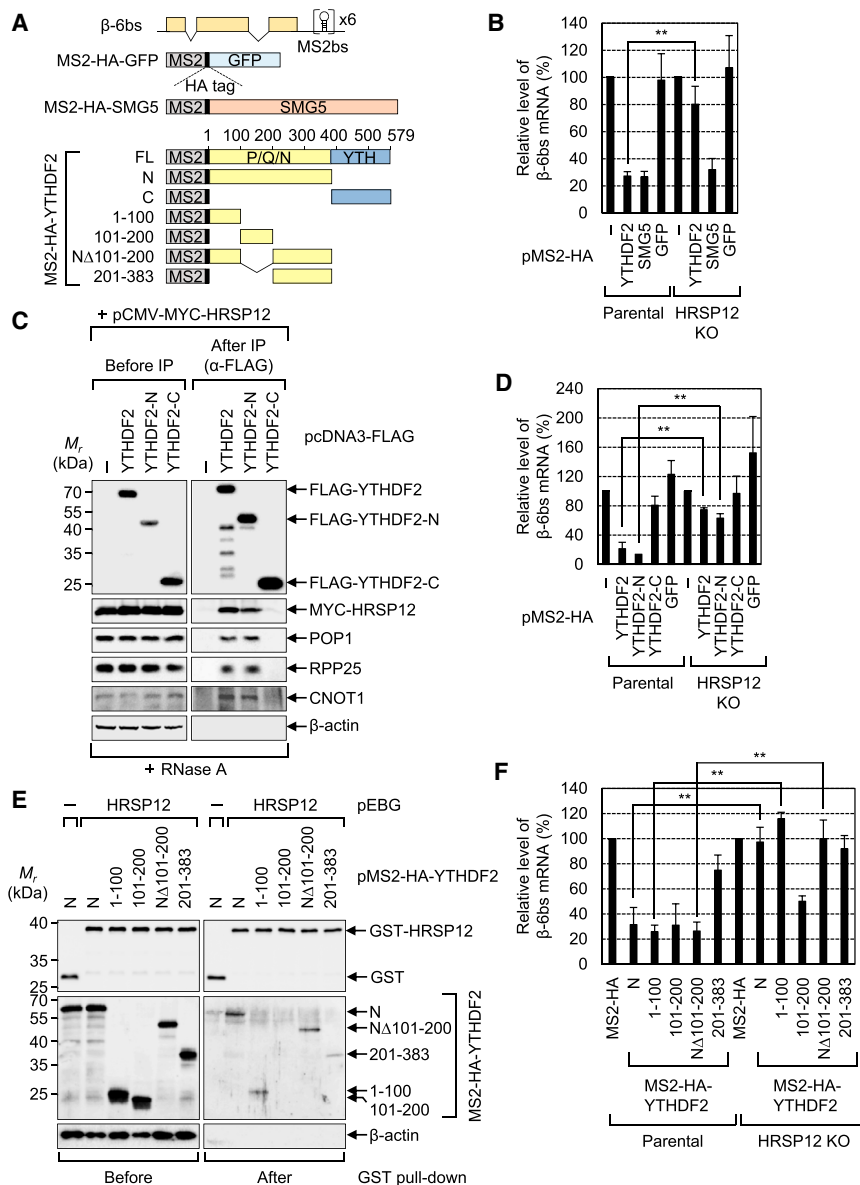
Figure 3. N-Terminal 100 aa of YTHDF2 Are a Minimal Region for Eliciting RNA Degradation via Its Binding to HRSP12

(A) Schematic representation of reporter mRNA and effector proteins used in our MS2/MS2bs tethering system. The β-6bs reporter mRNA contained six tandem repeats of the MS2bs in the 3′ UTR of the β-globin gene. Effector proteins were fused to MS2 followed by an HA tag. FL, full-length; P/Q/N, P/Q/N-rich low-complexity regions; YTH, YTH domain.

(B) Tethering experiments in parental or HRSP12-KO HAP1 cells. The cells were transiently transfected with a reporter plasmid, one of the effector plasmids, and a reference plasmid, phCMV-MUP. The levels of β-6bs mRNA were normalized to the levels of *MUP* mRNAs. The normalized levels of β-6bs mRNA in cells expressing MS2-HA were arbitrarily set to 100%. n = 3; **p < 0.01.

(C) IPs of YTHDF2 or its variants. IPs were carried out with an α-FLAG antibody and the extracts of cells expressing either FLAG-YTHDF2 or its variant. Total-cell extracts were treated with RNase A before IPs. n = 2.

(D) Artificial tethering of YTHDF2 or its variants. As performed in (B), except that MS2-HA-YTHDF2 or one of its variants was tethered. n = 3; **p < 0.01.

(E) A GST pull-down assay using GST-HRSP12 and MS2-HA-fused YTHDF2 variants. The extracts of cells expressing GST-HRSP12 and one of MS2-HA-fused YTHDF2 variants were treated with RNase A before GST pull-down. n = 2.

(F) Artificial tethering of YTHDF2 variants. n = 3; **p < 0.01.

and immunoprecipitation (PAR-CLIP) and a RNP-IP followed by next-generation sequencing (RIP-seq). According to the data from the PAR-CLIP and RIP-seq, HeLa cell transcripts were categorized into four groups: non-targets (absent from the PAR-CLIP and RIP-seq), CLIP–IP targets (present only in the PAR-CLIP but not in RIP-seq), CLIP targets (present in the PAR-CLIP), and CLIP∩IP targets (present in both the PAR-CLIP and RIP-seq).

A cumulative distribution function (CDF) analysis revealed that overall the CLIP–IP, CLIP, and CLIP∩IP targets significantly and gradually increased in abundance upon downregulation of YTHDF2, HRSP12, POP1, RPP20, or METTL3 (Figures 4A–4E and S4A–S4C), and their half-life increased after downregulation of YTHDF2, HRSP12, or POP1 (Figures 4G–4I) as compared with non-targets. In agreement of these results, the reanalysis of previously reported RNA-seq data from HRSP12-depleted HeLa cells (Park et al., 2016) and *RMRP* knockdown HeLa cells generated by targeted CRISPR-based disruption (Goldfarb and Cech, 2017) also revealed a significant increase in the abundance of CLIP–IP, CLIP, and CLIP∩IP targets after HRSP12 downregulation (Figure S4D) or *RMRP* downregulation (Figure S4E) in comparison with the control cells. Collectively, the data indicated that

the HRSP12-RNase P/MRP pathway is mechanistically separable from the CCR4-NOT1 pathway. Thus, we conclude that the N-terminal 1–100 aa of YTHDF2 represent a minimal region for HRSP12 binding and are sufficient for rapid RNA degradation with the help of HRSP12.

HRSP12 and RNase P/MRP Destabilize YTHDF2-Bound Transcripts at the Transcriptome Level

To investigate the effect of HRSP12 and RNase P/MRP at the transcriptome level, we carried out mRNA sequencing (mRNA-seq) experiments for measuring abundance (Figures 4A–4F; Tables S1A and S1B) and half-life (Figures 4G–4I; Table S1C) using total-RNA samples purified from HeLa cells either not depleted or depleted of the protein indicated in the figures. One research group (Wang et al., 2014) identified YTHDF2-binding transcripts in HeLa cells by photoactivatable ribonucleoside cross-linking
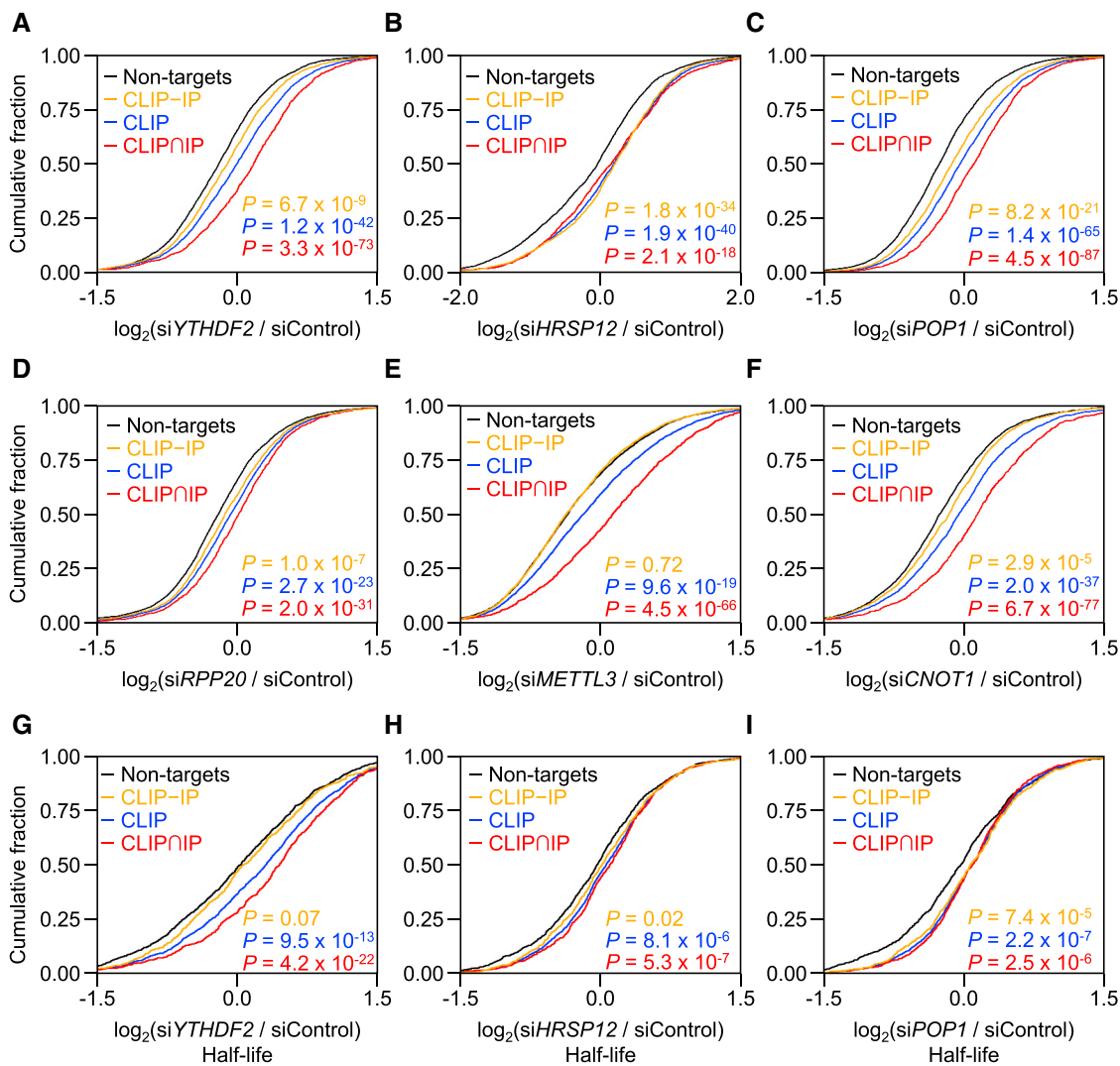
Figure 4. YTHDF2-Bound Transcripts Increase in Abundance and Half-Life after Downregulation of YTHDF2, HRSP12, or a Component of RNase P/MRP

(A–F) Cumulative distribution function (CDF) plots for the relative change in the abundance of transcripts. Total-RNA samples were purified and subjected to mRNA sequencing (n = 2). CDF plots of transcripts among non-targets (3,905), CLIP–IP targets (1,974), CLIP targets (3,250), and CLIP∩IP targets (1,276) were plotted as the relative changes in abundance of transcripts within each group after downregulation of YTHDF2 (A), HRSP12 (B), POP1 (C), RPP20 (D), METTL3 (E), or CNOT1 (F).

(G–I) CDF plots for the relative change in the half-life of transcripts. To determine the half-life of transcripts using HeLa cells depleted of the indicated protein, mRNA sequencing experiments were carried out as described in STAR Methods (n = 2). CDF plots of transcripts were built as relative changes in the half-life of transcripts within each group after downregulation of YTHDF2 (G), HRSP12 (H), or POP1 (I).

p values were calculated by the two-tailed Mann-Whitney U test.

HRSP12 and RNase P/MRP destabilize YTHDF2-bound transcripts at the transcriptome level.

It should be noted that significant upregulation of CLIP–IP, CLIP, and CLIP∩IP targets was also observed when CNOT1 was downregulated (Figure 4F). Double downregulation of HRSP12 and CNOT1 did not significantly affect the abundance of non-targets, CLIP, or CLIP∩IP transcripts as compared with single downregulation of either HRSP12 or CNOT1 (Figures S4F–S4I), suggesting that two RNA decay pathways mediated by the HRSP12-RNase P/MRP or CCR4-NOT complex are coupled to each other for efficient m^{6}A RNA decay.

HRSP12 Directly Binds to a Transcript and Elicits YTHDF2-Mediated RNA Decay

A recent effort to screen proteins for RNA-binding ones in HeLa cells identified HRSP12 as an RNA-binding protein (Castello et al., 2012). Therefore, to look for transcriptome-wide interactions between HRSP12 and target transcripts, we carried out cross-linking IP experiments coupled with high-throughput sequencing (CLIP-seq).

Raw reads obtained from two independent CLIP-seq experiments with HRSP12 (CLIP1 and CLIP2) were processed by adaptor sequence trimming, removal of ribosomal sequences,
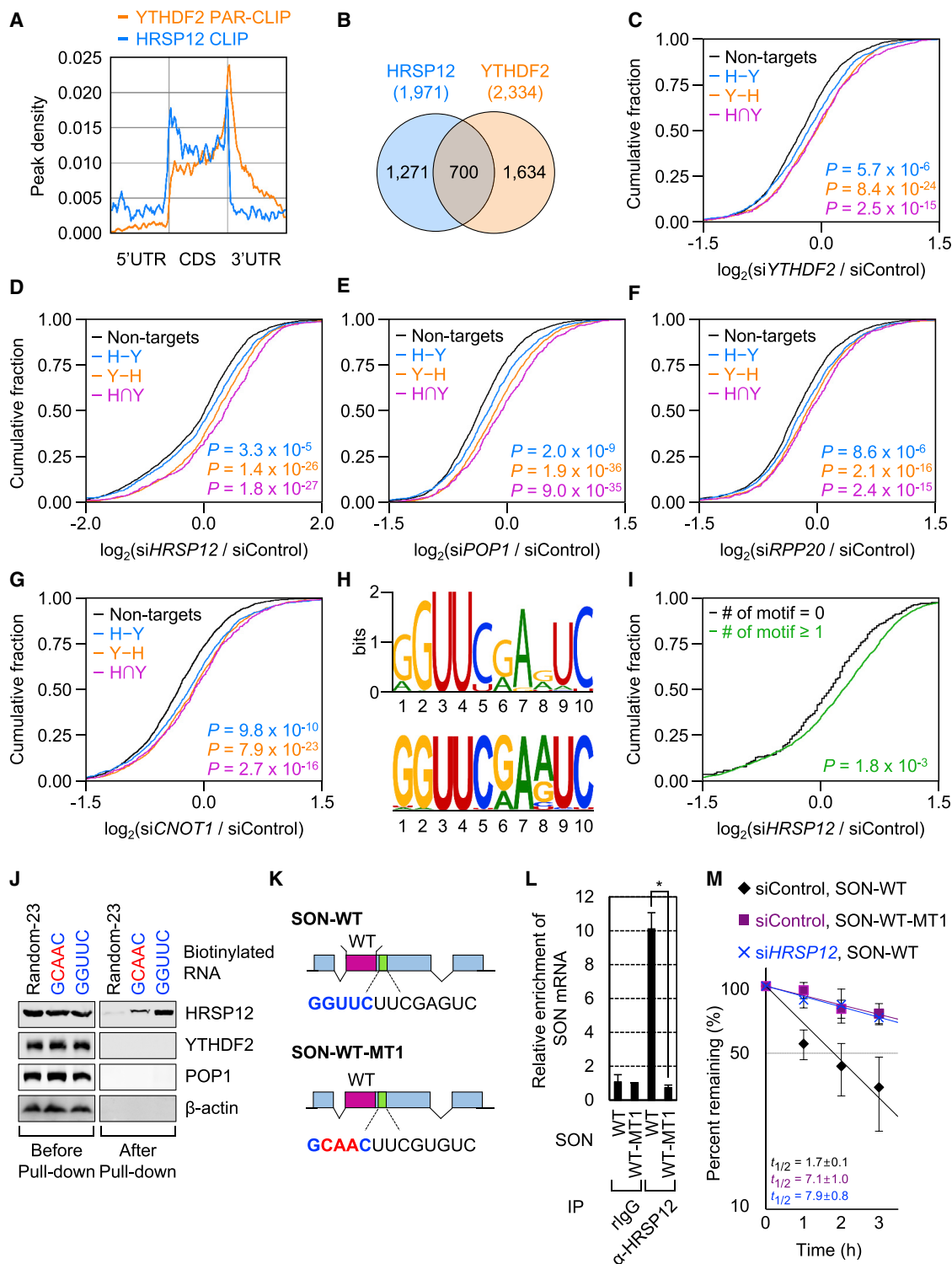
Figure 5. HRSP12 Directly Binds to a Transcript and Elicits Rapid RNA Degradation via the YTHDF2-HRSP12-RNase P/MRP Pathway

(A) Metagene profiles of the CLIP peaks of HRSP12 and YTHDF2 (Wang et al., 2014).

(B) Venn diagrams for the number of genes (abundance of transcripts: FPKM ≥ 5) containing HRSP12 peaks or YTHDF2 peaks.

(C–G) CDF plots of the relative changes in abundance of transcripts among non-targets (2,213), H–Y (1,271), Y–H (1,634), and H∩Y targets (700) after down-regulation of YTHDF2 (C), HRSP12 (D), POP1 (E), RPP20 (F), or CNOT1 (G).

(H) The logo of the consensus motif for HRSP12 binding. The consensus motif was discovered by MEME (upper, 3.4×10^{-30}) or HOMER (lower, p = 1.0×10^{-73}).

and mapping to the human reference genome sequence (hg19: Table S2). After a peak-calling process, we obtained 11,883 called peaks in CLIP1 and 18,703 called peaks in CLIP2. The Pearson correlation coefficient (r) between CLIP1 and CLIP2 for reads per million mapped reads (RPMs) of the common peaks (8,822) was 0.927, indicating a strong correlation between CLIP1 and CLIP2 (Figure S5A). When the number of peaks was adjusted for the nucleotide length of the regions, the majority of the peaks were preferentially enriched in 5′ UTRs and coding sequences (CDSs; Figure S5B).

Previously reported raw data from YTHDF2 PAR-CLIP (Wang et al., 2014) were also processed via PARalyzer, a PAR-CLIP peak-calling tool. Then, the relative densities of the peaks (3,264) obtained from HRSP12 CLIPs and the peaks (8,142) obtained from YTHDF2 CLIPs were compared by metagene analysis (Figure 5A). HRSP12 peaks were preferentially mapped to CDSs. In agreement with another report (Wang et al., 2014), the data processing through our pipeline revealed that YTHDF2 peaks were highly enriched in the 3′ end of CDSs.

As for the positions of the peaks, only 1.0% of all YTHDF2 peaks (105 out of 10,508 peaks) overlapped with all HRSP12 peaks obtained from two biological replicates (105 out of 21,885 peaks), indicating that most YTHDF2 peaks do not overlap with HRSP12 peaks. On the other hand, a comparison of the genes containing an HRSP12 peak (obtained from two biological replicates of HRSP12 CLIP) or YTHDF2 peak (Wang et al., 2014)—after application of a fragment per kilobase of transcript per million mapped reads (FPKM) filtering cutoff of 5 to the abundance of transcripts—revealed that 1,971 and 2,334 genes had the peak for HRSP12 and YTHDF2, respectively (Figure 5B). Among these, 700 genes were in the overlap between HRSP12 CLIP and YTHDF2 CLIP. We next categorized the transcripts into three groups: non-targets (2,213; absent from both HRSP12 CLIP and YTHDF2 CLIP), H–Y targets (1,271; present only in the HRSP12 CLIP), Y–H only targets (1,634; present only in the YTHDF2 CLIP), and H∩Y targets (700; present in both the HRSP12 CLIP and YTHDF2 CLIP). The CDF analysis uncovered a significant and gradual increase in the abundance of H–Y, Y–H, and H∩Y targets after downregulation of YTHDF2, HRSP12, POP1, RPP20, or CNOT1 (Figures 5C–5G). Consistent with these results, the reanalysis of previously reported RNA-seq data from HeLa cells depleted of HRSP12 (Park et al., 2016) or *RMRP* RNA (Goldfarb and Cech, 2017) also indicated that H–Y, Y–H, and H∩Y targets were gradually upregulated upon downregulation of HRSP12 (Figure S5C) or *RMRP* (Figure S5D). Furthermore, HRSP12-bound m⁶A transcripts more significantly increased in abundance when YTHDF2, HRSP12, POP1, RPP20, or CNOT1 were downregulated, as compared with HRSP12-bound nonmethylated transcripts (Figures S5E–S5J). All these

data indicated that HRSP12 directly binds to and destabilizes m⁶A transcripts via YTHDF2 and RNase P/MRP at the transcriptome level.

Consensus motif analysis of the peaks among the 1,971 genes common for the CLIP1 and CLIP2 experiments on HRSP12 revealed GGUUC as the most predominant RNA motif for HRSP12 (Figure 5H). Interestingly, the identified GGUUC motif was located in the 5′ half of a potential palindromic sequence. Comparative analysis revealed that, among YTHDF2 targets (2,334 genes), the transcripts (2,081) with one or more motifs were significantly upregulated upon downregulation of HRSP12, as compared with transcripts lacking the motif (253; Figure 5I). The number of the motifs correlated with upregulation of transcripts after the downregulation of HRSP12 with weak significance (Figure S5K). Direct binding of HRSP12 to the GGUUC motif was demonstrated by in vitro CLIP experiments with biotinylated probes (Figure 5J), which allow for measuring a direct protein-RNA interaction (Castello et al., 2012). The substitution of GGUUC with GCAAC disrupted the binding of HRSP12. In addition, we found that the SON reporter mRNA contained the consensus sequence that matched the identified HRSP12-binding motif downstream of m⁶A sites (Figure 5K). In vivo CLIP experiments, which allow for monitoring a direct protein-RNA interaction within the cell (Murigneux et al., 2013), showed that SON reporter mRNA harboring GGUUC, but not its variant GCAAC, was preferentially enriched in HRSP12 CLIP (Figure 5L). In addition, substitution of GGUUC with GCAAC increased the half-life of SON reporter mRNA (Figure 5M), suggesting that direct binding of HRSP12 to the motif promotes m⁶A-mediated mRNA decay.

m⁶A-Containing Transcripts Are Endoribonucleolytically Cleaved in a Way that Depends on HRSP12 and RNase P/MRP

Although one report showed that HRSP12 has an endoribonuclease activity (Morishita et al., 1999), purified recombinant HRSP12 and HRSP12(P105A/R107E) failed to cleave RNA substrates under our conditions (Figure S6A). Considering that HRSP12 links YTHDF2 and RNase P/MRP in vivo and in vitro (Figure 1), we tested whether m⁶A transcripts could be targeted for RNase P/MRP-mediated endoribonucleolytic cleavage. To this end, we designed specific oligonucleotides for amplification of different regions of SON reporter mRNAs (Figure S6B). To stabilize 3′ intermediate fragments, HeLa cells that were either depleted or not depleted of POP1 were simultaneously depleted of both cytoplasmic and nuclear 5′-to-3′ exoribonucleases: XRN1 and XRN2 (XRN1/2). The amounts of all the tested fragments of SON-WT reporter mRNA effectively decreased in a POP1-dependent manner (Figures S6C and S6D). Intriguingly,

(I) CDF plots of the relative changes in abundance of transcripts without (253 genes) or with (2,081 genes) the consensus motif (GGUUC) among YTHDF2 CLIP targets (2,334) after downregulation of HRSP12.

(J) In vitro CLIP by means of a biotinylated probe harboring the HRSP12-binding motif (GGUUC) or its mutant variant (GCAAC). A biotinylated random 23-mer RNA probe served as a control. n = 3.

(K) Schematic representation of m⁶A reporter mRNAs: SON-WT and SON-WT-MT1. The HRSP12-binding motif and the mutated sequences are indicated in blue and red, respectively.

(L) In vivo CLIP of HRSP12 using SON reporter mRNAs. n = 3.

(M) Half-life of SON reporter mRNAs in the cells either not depleted or depleted of HRSP12. n = 3.

downregulation of XRN1/2 significantly reversed the observed reduction in the level of the 3′-1 and 3′-2 fragments of SON-WT reporter mRNA, without affecting the level of the 3′-3 fragment, 5′ fragment, and the full-length reporter mRNA (Figure S6D), indicating that RNase P/MRP cleaves a region 0–60 nucleotides downstream of the HRSP12-binding site in SON reporter mRNA. Similar experiments using HAP1 cells, either parental or HRSP12-KO (Figures S6E and S6F), also suggested that HRSP12 elicits endoribonucleolytic cleavage of m6A mRNA.

The HRSP12-Binding Site and RNase P/MRP Cleavage Site Are Mostly Located Upstream and Downstream, Respectively, of the YTHDF2-Binding Site

To identify the exact positions of endoribonucleolytic sites cleaved by RNase P/MRP within YTHDF2-bound transcripts at a transcriptome level, we applied parallel analysis of RNA ends sequencing (PARE-seq), which enables determination of the 5′ end of 3′ intermediate fragments generated by endoribonucleolytic cleavage (German et al., 2008; Schmidt et al., 2015). To stabilize 3′ intermediate fragments, HeLa cells were depleted of XRN1/2. To select 3′ intermediate fragments dependent on YTHDF2, HRSP12, and RNase P/MRP, the cells were simultaneously depleted of XRN1/2 and YTHDF2, HRSP12, or POP1. From two biological replicates (PARE1 and PARE2) of PARE-seq analysis of HeLa cells depleted of XRN1/2, we obtained 21,978 and 10,648 PARE sequences, respectively (tags per 5 million [TP5M] $\geq$ 100; Table S3). Among these, the read abundance levels of 16,250 and 6,862 PARE sequences, respectively, commonly decreased more than 2-fold after downregulation of YTHDF2, HRSP12, or POP1. After a FPKM filtering cutoff of 5 was applied to the abundance of transcripts, we obtained 13,105 and 5,284 PARE sequences (covering 4,471 and 2,927 genes, respectively) as cleavage sites dependent on YTHDF2, HRSP12, and RNase P/MRP. After that, the 5′ ends of the most abundant PARE sequences among those obtained from PARE1 and PARE2 were defined as PARE MaxSeqs. Nucleotide composition analysis of the 10-nucleotide region surrounding 2,257 MaxSeqs revealed no sequence preference for cleavage (Figure 6A), suggesting that the YTHDF2-HRSP12-RNase P/MRP pathway performs cleavage of target substrates in a sequence-independent manner. The majority of the MaxSeqs were enriched in both CDSs and 3′ UTRs (Figure S6G), with the highest density around the translation termination codon in metagene analysis (Figure 6B).

We next compared the genes obtained in HRSP12 CLIP, YTHDF2 CLIP, and PARE experiments and found that 328 (47%) out of the 700 genes in the overlap between HRSP12 CLIP and YTHDF2 CLIP (Figure 5B) were shared with the genes of PARE (Figure 6C). The set of 328 transcripts was found to be significantly enriched with various biological and molecular terms of Gene Ontology (Table S4). From the 328 common genes, the most abundant CLIP peaks (MaxPeaks) and PARE MaxSeqs were selected. Then, the distances between the centers of an HRSP12 MaxPeak and a PARE MaxSeq relative to the center of a YTHDF MaxPeak in individual mRNAs (115; Figure 6D) were plotted (see also Table S5 for genomic positions). Overall, HRSP12 MaxPeaks turned out to be positioned upstream of YTHDF2 MaxPeaks (Figure 6D) and m6A MaxPeaks

(Figure S6H) in mRNAs (the medians of the distance were 862 and 591 nucleotides, respectively). In contrast, PARE MaxSeqs were positioned downstream of YTHDF2 MaxPeaks in mRNAs (the median of the distance was 421 nucleotides). In addition, the metagene analysis of a MaxPeak and MaxSeq in individual mRNAs uncovered similar distribution patterns (Figure 6E). Of note, none of the PARE MaxSeqs was observed in the 5′ UTR. Taken together, these data indicated that there is a significant propensity of HRSP12 to bind upstream of a YTHDF2-binding site and that RNase P/MRP preferentially cleaves RNA downstream of a YTHDF2-binding site. The observed long-range interaction between HRSP12 and YTHDF2 and the presence of the cleavage sites several hundred nucleotides downstream of a YTHDF2-binding site may be achieved by long-range RNA looping. Indeed, we found that the common mRNAs were significantly longer than cellular mRNAs on average (Figure 6F).

Next, we assessed the relative change in the half-life of transcripts when a specific factor was downregulated. Cellular transcripts were categorized into three groups: non-targets (1,576, absent from HRSP12 CLIP, YTHDF2 CLIP, and PARE-seq), H∩Y targets (700, common targets of both HRSP12 CLIP and YTHDF2 CLIP), and H∩Y∩P targets (328, common targets of HRSP12-CLIP, YTHDF2 CLIP, and PARE-seq). The CDF analysis showed that the half-life of both H∩Y and H∩Y∩P targets significantly increased when YTHDF2, HRSP12, or POP1 was downregulated (Figures 6G–6I), indicating that transcripts commonly bound by YTHDF2 and HRSP12 are preferential cellular substrates for RNase P/MRP-dependent degradation.

HRSP12 and YTHDF2 Cooperatively Work to Help Each Other to Bind to mRNA

Our observations of a long-range interplay between HRSP12 and YTHDF2 (Figure 6) led us to wonder whether these two proteins affect each other's RNA binding. For this purpose, we employed in vivo CLIP experiments (Figures 7A–7D and S7A–S7D). The results showed that downregulation of YTHDF2 inhibited the direct binding of HRSP12 to SON-WT reporter mRNA relative to Mut mRNA (Figure 7A) and vice versa (Figure 7B), indicating that HRSP12 cooperates with YTHDF2 for mRNA binding. Of note, POP1 downregulation did not significantly affect direct binding of HRSP12 or YTHDF2 to mRNA (Figures 7C and 7D), although POP1 efficiently associated with WT reporter mRNA (Figures S7E and S7F). The observed cooperativity between HRSP12 and YTHDF2 in terms of RNA binding within the cell was further confirmed by in vitro CLIP with biotinylated probes harboring either the HRSP12-binding motif (GGUUC) or not (GCAAC) and harboring either a nonmethylated (A) or m6A site (Figures 7E).

Circular RNAs (circRNAs) Associating with YTHDF2 in an HRSP12-Dependent Manner Are Preferentially Downregulated by RNase P/MRP

We next employed circRNAs, the majority of which are generated as a consequence of back splicing of internal exons (Chen, 2016). Because circRNAs lack free 5′ and 3′ ends, endoribonucleolytic cleavage is the only way to degrade circRNAs. We first tested whether the previously characterized 11 m6A-containing circRNAs (Yang et al., 2017; Zhou et al., 2017) associate with YTHDF2 (Figures 7F and S7G). Among them, seven circRNAs
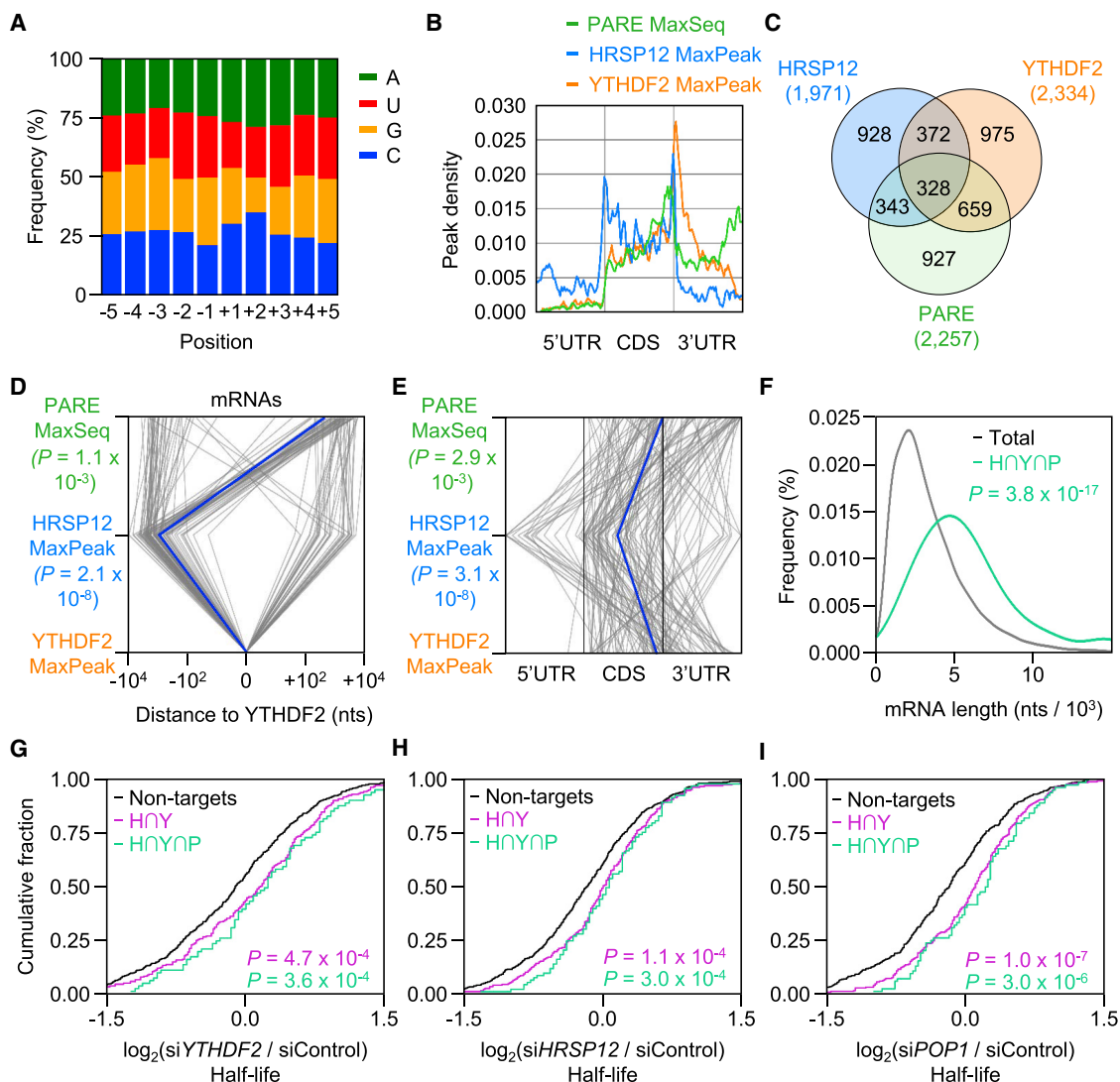
Figure 6. Transcripts Bound by Both HRSP12 and YTHDF2 Are Preferably Cleaved Downstream of the YTHDF2-Binding Site by RNase P/MRP

(A) Nucleotide composition analysis of the 10-nucleotide region surrounding PARE MaxSeqs (2,257), where the cleavages were commonly dependent on YTHDF2, HRSP12, and POP1.

(B) Metagene profiles of PARE MaxSeq, HRSP12 MaxPeak, and YTHDF2 MaxPeak.

(C) Venn diagrams for the number of genes (abundance of transcripts: FPKM ≥ 5) containing PARE MaxSeq, HRSP12 MaxPeak, or YTHDF2 MaxPeak.

(D) Distance profiles of PARE MaxSeq, HRSP12 MaxPeak, and YTHDF2 MaxPeak in individual mRNAs (115). p values were calculated by the one-tailed Mann–Whitney U test.

(E) Metagene profiles of the positions of PARE MaxSeq, HRSP12 MaxPeak, and YTHDF2 MaxPeak in an individual mRNA (115). p values were calculated by the one-tailed Mann–Whitney U test.

(F) Length distribution of total-cell mRNAs (19,288) and common mRNAs (115).

(G–I) CDF plots of relative changes in the half-life of transcripts among non-targets (1,576), H∩Y targets (700), and H∩Y∩P targets (328) after downregulation of the indicated protein. p values were calculated by the two-tailed Mann–Whitney U test.

were found to be significantly enriched in the immunoprecipitate of YTHDF2. The observed enrichment with three (*cMATR3*, *cFAM20B*, and *cSLC45A4*) out of the seven circRNAs was significantly reversed by HRSP12 downregulation (Figure 7F). Notably, only the three out of all tested 11 circRNAs commonly increased in abundance after downregulation of YTHDF2, HRSP12, or POP1 (Figures 7G and S7H), indicating that circRNAs associ-

ating with YTHDF2 in an HRSP12-dependent manner are endoribonucleolytically cleaved by RNase P/MRP.

DISCUSSION

Recent cumulative data revealed that m6A modification plays a regulatory role in a wide range of biological and physiological
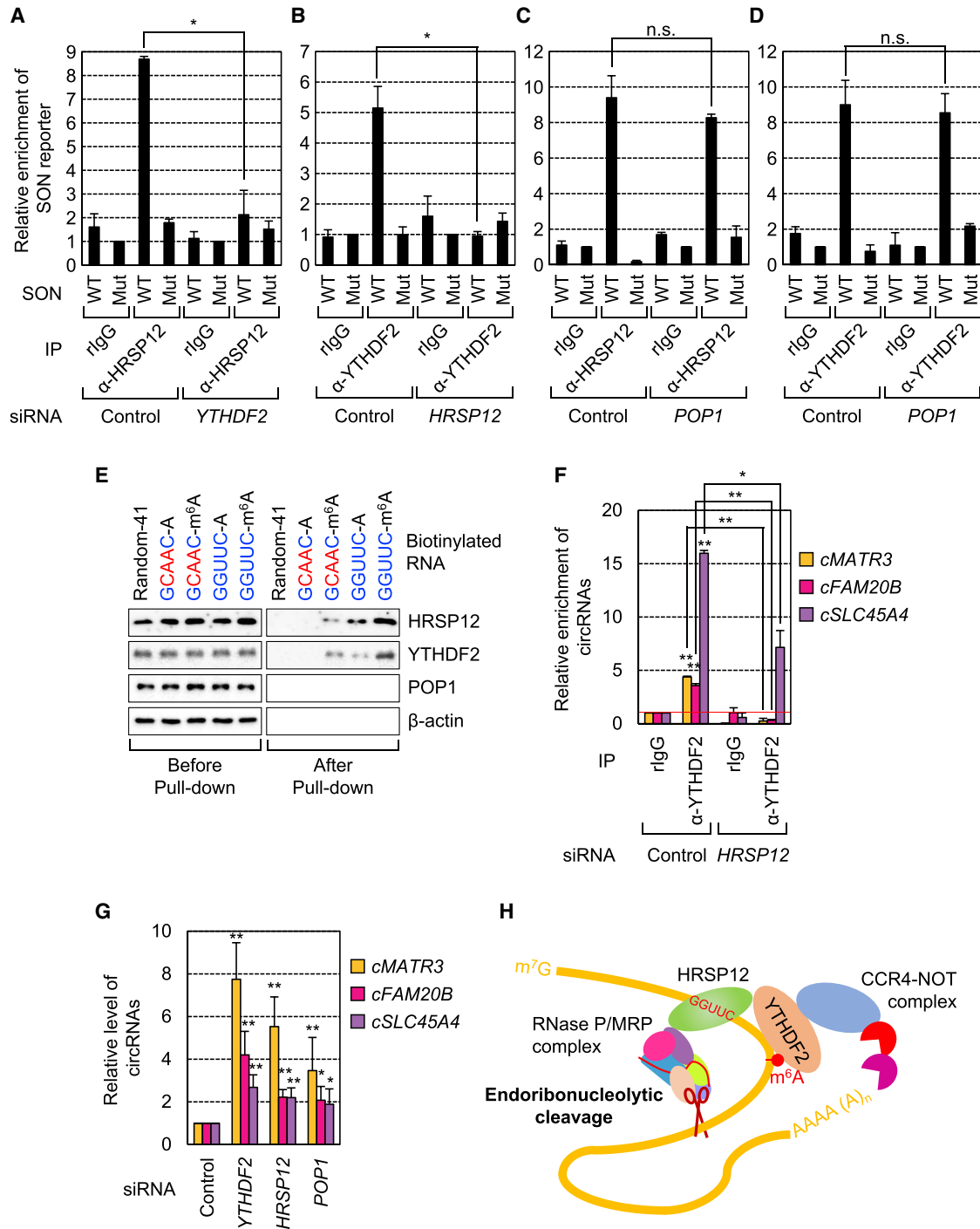
Figure 7. Cooperative Binding of HRSP12 and YTHDF2 to m⁶A RNA Contributes to Endoribonucleolytic Cleavage of a Subset of m⁶A-Containing Circular RNAs

(A–D) *In vivo* CLIPs of HRSP12 or YTHDF2. HeLa cells depleted of YTHDF2 (A), HRSP12 (B), or POP1 (C and D) were cotransfected with one of the SON reporter plasmids and with phCMV-MUP as a reference plasmid. The extracts of the cells were subjected to in vivo CLIPs using either α-HRSP12 antibody (A and C) or α-YTHDF2 antibody (B and D). The relative levels of Mut reporter mRNAs in CLIP using rIgG were arbitrarily set to 100%. n = 3; *p < 0.05; n.s.: not significant.

(E) *In vitro* CLIP using a biotinylated probe harboring either the HRSP12-binding motif (GGUUC) or its mutant variant (GCAAC) and harboring either nonmethylated (A) or m⁶A site. A biotinylated random 41-mer RNA probe served as a control. n = 3.

(legend continued on next page)

processes. Despite its important functions, the molecular details of how m⁶A RNAs are degraded by binding to YTHDF2 are still unclear. Here, we describe endoribonucleolytic cleavage of m⁶A RNAs via a YTHDF2-HRSP12-RNase-P/MRP pathway (Figure 7H).

Our transcriptome-wide characterization of HRSP12-binding sites (Figure 5) and cleavage sites of RNase P/MRP (Figure 6) suggests that HRSP12 mostly binds to m⁶A mRNAs approximately 862 nucleotides (a median value) upstream of YTHDF2-binding sites and that RNase P/MRP mostly cleaves approximately 421 nucleotides (a median value) downstream of a YTHDF2-binding site within m⁶A RNAs. How does HRSP12 located far upstream of YTHDF2 affect mRNA stability? One possible explanation can be found in a long-range interaction within eukaryotic mRNAs (Jackson et al., 2010). For instance, a cap structure at the 5′ end can communicate with a poly(A) structure (poly(A) tail) at the 3′ end of mRNAs to modulate translation efficiency via cooperative binding of eukaryotic translation initiation factor 4F and poly(A)-binding protein to mRNAs (Safaee et al., 2012). Analogously to the long-range interaction observed in eukaryotic mRNAs, the upstream HRSP12 may cooperatively work with the downstream YTHDF2 for their binding to mRNA. Indeed, we observed increased association between YTHDF2 and m⁶A-containing linear and circular RNAs via HRSP12 (Figure 7).

Our observations reveal complexities in the regulation of stability of m⁶A-containing RNAs. The YTHDF2-bound m⁶A RNAs may be degraded by at least two pathways: if the RNAs contain HRSP12-binding sites, these RNAs will be preferentially degraded by RNase P/MRP-mediated endoribonucleolytic pathways coupled to the CCR4-NOT complex-mediated deadenylation pathway via cooperative binding of HRSP12 and YTHDF2 to m⁶A mRNAs (Figure 7), as demonstrated by double downregulation of HRSP12 and CNOT1 (Figures S4F–S4I). Although YTHDF2-bound m⁶A RNAs lack HRSP12-binding sites, YTHDF2 may still interact with HRSP12 and elicit both decay pathways with lesser efficiency (Figures 4, 5, and 6). In addition to the two aforementioned pathways, the presence of additional routes for m⁶A RNA decay is implied by a recent report showing that YTHDF1, YTHDF2, and YTHDF3 share common targets among m⁶A RNAs and cooperatively affect the stability of common targets (Shi et al., 2017). Thus, we speculate that the complexities in degradation of m⁶A RNAs contribute to more dynamic regulation of m⁶A RNA during various biological and physiological processes involving m⁶A modification.

STAR★METHODS

Detailed methods are provided in the online version of this paper and include the following:

- KEY RESOURCES TABLE
- CONTACT FOR REAGENT AND RESOURCE SHARING

- EXPERIMENTAL MODEL AND SUBJECT DETAILS
- METHOD DETAILS
  - Plasmid construction
  - DNA or siRNA transfection
  - Protein expression and purification
  - Antibodies
  - Quantitative real-time RT-PCR
  - Measurement of mRNA half-life
  - Immunoprecipitation
  - *In vitro* GST pull-down assay
  - *In vitro* CLIP using biotinylated RNAs
  - *In vivo* CLIP
  - *In vitro* RNA cleavage assay
  - Far-western blotting
  - Nucleocytoplasmic fractionation
  - mRNA sequencing
  - CLIP sequencing (CLIP-seq)
  - PARE sequencing (PARE-seq)
  - General processing and mapping of reads
  - Transcriptome analysis and RNA half-life profiling
  - CLIP peak calling and analysis
  - Metagene analysis
  - Consensus motif analysis
  - m⁶A-seq analysis
  - PARE analysis
  - CDF analysis
  - Relative distances between CLIP MaxPeaks and PARE MaxSeqs
  - mRNA length distribution
- QUANTIFICATION AND STATISTICAL ANALYSIS
- DATA AND SOFTWARE AVAILABILITY

AUTHOR CONTRIBUTIONS

O.H.P., H.H., and Y.K.K. conceived and designed the experiments. H.H. analyzed the sequencing data. O.H.P., Y.L., and S.H.B. conducted the

(F) IPs of YTHDF2 in HeLa cells either not depleted or depleted of HRSP12. The amounts of coIPed endogenous circRNAs were normalized to the level of endogenous *GAPDH* mRNA. Then, the normalized levels obtained in IPs with rIgG in undepleted cells were arbitrarily set to 1.0. n = 3; *p < 0.05; **p < 0.01.
(G) The levels of endogenous circRNAs upon downregulation of the indicated proteins. The relative levels of circRNAs, normalized to the level of endogenous *GAPDH* mRNA, in undepleted cells were arbitrarily set to 1.0. n = 3; *p < 0.05; **p < 0.01.
(H) A proposed model for m⁶A mRNA decay via the YTHDF2-HRSP12-RNase P/MRP pathway. See the Discussion section for details.

experiments. D.H.K. purified the recombinant proteins under the supervision of H.K.S. and Y.K.K. O.H.P., H.H., and Y.K.K. wrote the manuscript.

REFERENCES

Alarcón, C.R., Goodarzi, H., Lee, H., Liu, X., Tavazoie, S., and Tavazoie, S.F. (2015). HNRNPA2B1 is a mediator of m(6)A-dependent nuclear RNA processing events. Cell *162*, 1299–1308.

Anders, S., Pyl, P.T., and Huber, W. (2015). HTSeq–a Python framework to work with high-throughput sequencing data. Bioinformatics *31*, 166–169.

Blomen, V.A., Májek, P., Jae, L.T., Bigenzahn, J.W., Nieuwenhuis, J., Staring, J., Sacco, R., van Diemen, F.R., Olk, N., Stukalov, A., et al. (2015). Gene essentiality and synthetic lethality in haploid human cells. Science *350*, 1092–1096.

Carette, J.E., Raaben, M., Wong, A.C., Herbert, A.S., Obernosterer, G., Mulherkar, N., Kuehne, A.I., Kranzusch, P.J., Griffin, A.M., Ruthel, G., et al. (2011). Ebola virus entry requires the cholesterol transporter Niemann-Pick C1. Nature *477*, 340–343.

Castello, A., Fischer, B., Eichelbaum, K., Horos, R., Beckmann, B.M., Strein, C., Davey, N.E., Humphreys, D.T., Preiss, T., Steinmetz, L.M., et al. (2012). Insights into RNA biology from an atlas of mammalian mRNA-binding proteins. Cell *149*, 1393–1406.

Chen, L.L. (2016). The biogenesis and emerging roles of circular RNAs. Nat. Rev. Mol. Cell Biol. *17*, 205–211.

Cho, H., Han, S., Choe, J., Park, S.G., Choi, S.S., and Kim, Y.K. (2013). SMG5-PNRC2 is functionally dominant compared with SMG5-SMG7 in mammalian nonsense-mediated mRNA decay. Nucleic Acids Res. *41*, 1319–1328.

Cho, H., Park, O.H., Park, J., Ryu, I., Kim, J., Ko, J., and Kim, Y.K. (2015). Glucocorticoid receptor interacts with PNRC2 in a ligand-dependent manner to recruit UPF1 for rapid mRNA degradation. Proc. Natl. Acad. Sci. USA *112*, E1540–E1549.

Corcoran, D.L., Georgiev, S., Mukherjee, N., Gottwein, E., Skalsky, R.L., Keene, J.D., and Ohler, U. (2011). PARalyzer: definition of RNA binding sites from PAR-CLIP short-read sequence data. Genome Biol. *12*, R79.

Coughlin, D.J., Pleiss, J.A., Walker, S.C., Whitworth, G.B., and Engelke, D.R. (2008). Genome-wide search for yeast RNase P substrates reveals role in maturation of intron-encoded box C/D small nucleolar RNAs. Proc. Natl. Acad. Sci. USA *105*, 12218–12223.

Dobin, A., Davis, C.A., Schlesinger, F., Drenkow, J., Zaleski, C., Jha, S., Batut, P., Chaisson, M., and Gingeras, T.R. (2013). STAR: ultrafast universal RNA-seq aligner. Bioinformatics *29*, 15–21.

Dominissini, D., Moshitch-Moshkovitz, S., Schwartz, S., Salmon-Divon, M., Ungar, L., Osenberg, S., Cesarkas, K., Jacob-Hirsch, J., Amariglio, N., Kupiec, M., et al. (2012). Topology of the human and mouse m6A RNA methylomes revealed by m6A-seq. Nature *485*, 201–206.

Du, H., Zhao, Y., He, J., Zhang, Y., Xi, H., Liu, M., Ma, J., and Wu, L. (2016). YTHDF2 destabilizes m(6)A-containing RNA through direct recruitment of the CCR4-NOT deadenylase complex. Nat. Commun. *7*, 12626.

Elefsinioti, A., Sarac, O.S., Hegele, A., Plake, C., Hubner, N.C., Poser, I., Sarov, M., Hyman, A., Mann, M., Schroeder, M., et al. (2011). Large-scale de novo prediction of physical protein-protein association. Mol. Cell Proteomics *10*, M111.010629.

Fu, Y., Dominissini, D., Rechavi, G., and He, C. (2014). Gene expression regulation mediated through reversible m6A RNA methylation. Nat. Rev. Genet. *15*, 293–306.

German, M.A., Pillay, M., Jeong, D.H., Hetawal, A., Luo, S., Janardhanan, P., Kannan, V., Rymarquis, L.A., Nobuta, K., German, R., et al. (2008). Global identification of microRNA-target RNA pairs by parallel analysis of RNA ends. Nat. Biotechnol. *26*, 941–946.

Goldfarb, K.C., and Cech, T.R. (2017). Targeted CRISPR disruption reveals a role for RNase MRP RNA in human preribosomal RNA processing. Genes Dev. *31*, 59–71.

Jackson, R.J., Hellen, C.U., and Pestova, T.V. (2010). The mechanism of eukaryotic translation initiation and principles of its regulation. Nat. Rev. Mol. Cell Biol. *11*, 113–127.

Jarrous, N. (2017). Roles of RNase P and its subunits. Trends Genet. *33*, 594–603.

Jia, G., Fu, Y., Zhao, X., Dai, Q., Zheng, G., Yang, Y., Yi, C., Lindahl, T., Pan, T., Yang, Y.G., and He, C. (2011). N6-methyladenosine in nuclear RNA is a major substrate of the obesity-associated FTO. Nat. Chem. Biol. *7*, 885–887.

Krogan, N.J., Cagney, G., Yu, H., Zhong, G., Guo, X., Ignatchenko, A., Li, J., Pu, S., Datta, N., Tikuisis, A.P., et al. (2006). Global landscape of protein complexes in the yeast Saccharomyces cerevisiae. Nature *440*, 637–643.

Li, A., Chen, Y.S., Ping, X.L., Yang, X., Xiao, W., Yang, Y., Sun, H.Y., Zhu, Q., Baidya, P., Wang, X., et al. (2017). Cytoplasmic m6A reader YTHDF3 promotes mRNA translation. Cell Res. *27*, 444–447.

Maida, Y., Yasukawa, M., Furuuchi, M., Lassmann, T., Possemato, R., Okamoto, N., Kasim, V., Hayashizaki, Y., Hahn, W.C., and Masutomi, K. (2009). An RNA-dependent RNA polymerase formed by TERT and the RMRP RNA. Nature *461*, 230–235.

Meyer, K.D., and Jaffrey, S.R. (2017). Rethinking m6A readers, writers, and erasers. Annu. Rev. Cell Dev. Biol. *33*, 319–342.

Meyer, K.D., Saletore, Y., Zumbo, P., Elemento, O., Mason, C.E., and Jaffrey, S.R. (2012). Comprehensive analysis of mRNA methylation reveals enrichment in 3′ UTRs and near stop codons. Cell *149*, 1635–1646.

Meyer, K.D., Patil, D.P., Zhou, J., Zinoviev, A., Skabkin, M.A., Elemento, O., Pestova, T.V., Qian, S.B., and Jaffrey, S.R. (2015). 5′ UTR m(6)A promotes cap-independent translation. Cell *163*, 999–1010.

Morishita, R., Kawagoshi, A., Sawasaki, T., Madin, K., Ogasawara, T., Oka, T., and Endo, Y. (1999). Ribonuclease activity of rat liver perchloric acid-soluble protein, a potent inhibitor of protein synthesis. J. Biol. Chem. *274*, 20688–20692.

Murigneux, V., Saulière, J., Roest Crollius, H., and Le Hir, H. (2013). Transcriptome-wide identification of RNA binding sites by CLIP-seq. Methods *63*, 32–40.

Park, O.H., Park, J., Yu, M., An, H.T., Ko, J., and Kim, Y.K. (2016). Identification and molecular characterization of cellular factors required for glucocorticoid receptor-mediated mRNA decay. Genes Dev. *30*, 2093–2105.

Roundtree, I.A., Evans, M.E., Pan, T., and He, C. (2017a). Dynamic RNA modifications in gene expression regulation. Cell *169*, 1187–1200.

Roundtree, I.A., Luo, G.Z., Zhang, Z., Wang, X., Zhou, T., Cui, Y., Sha, J., Huang, X., Guerrero, L., Xie, P., et al. (2017b). YTHDC1 mediates nuclear export of N6-methyladenosine methylated mRNAs. eLife *6*, e31311.

Ryu, I., Won, Y.-S., Ha, H., Kim, E., Park, Y., Kim, M.K., Kwon, D.H., Choe, J., Song, H.K., Jung, H., and Kim, Y.K. (2019). eIF4A3 phosphorylation by CDKs affects NMD during the cell cycle. Cell Rep. *26*, 2126–2139.

Safaee, N., Kozlov, G., Noronha, A.M., Xie, J., Wilds, C.J., and Gehring, K. (2012). Interdomain allostery promotes assembly of the poly(A) mRNA complex with PABP and eIF4G. Mol. Cell *48*, 375–386.

Schmidt, S.A., Foley, P.L., Jeong, D.H., Rymarquis, L.A., Doyle, F., Tenenbaum, S.A., Belasco, J.G., and Green, P.J. (2015). Identification of SMG6 cleavage sites and a preferred RNA cleavage motif by global analysis of endogenous NMD targets in human cells. Nucleic Acids Res. *43*, 309–323.

Schmieder, R., Lim, Y.W., and Edwards, R. (2012). Identification and removal of ribosomal RNA sequences from metatranscriptomes. Bioinformatics *28*, 433–435.

Shi, H., Wang, X., Lu, Z., Zhao, B.S., Ma, H., Hsu, P.J., Liu, C., and He, C. (2017). YTHDF3 facilitates translation and decay of N[6]-methyladenosine-modified RNA. Cell Res. *27*, 315–328.

Wang, X., Lu, Z., Gomez, A., Hon, G.C., Yue, Y., Han, D., Fu, Y., Parisien, M., Dai, Q., Jia, G., et al. (2014). N6-methyladenosine-dependent regulation of messenger RNA stability. Nature *505*, 117–120.

Wang, X., Zhao, B.S., Roundtree, I.A., Lu, Z., Han, D., Ma, H., Weng, X., Chen, K., Shi, H., and He, C. (2015). N(6)-methyladenosine modulates messenger RNA translation efficiency. Cell *161*, 1388–1399.

Wilusz, J.E., Freier, S.M., and Spector, D.L. (2008). 3′ end processing of a long nuclear-retained noncoding RNA yields a tRNA-like cytoplasmic RNA. Cell *135*, 919–932.

Xiao, W., Adhikari, S., Dahal, U., Chen, Y.S., Hao, Y.J., Sun, B.F., Sun, H.Y., Li, A., Ping, X.L., Lai, W.Y., et al. (2016). Nuclear m(6)A reader YTHDC1 regulates mRNA splicing. Mol. Cell *61*, 507–519.

Yang, Y., Fan, X., Mao, M., Song, X., Wu, P., Zhang, Y., Jin, Y., Yang, Y., Chen, L.L., Wang, Y., et al. (2017). Extensive translation of circular RNAs driven by N[6]-methyladenosine. Cell Res. *27*, 626–641.

Yang, Y., Hsu, P.J., Chen, Y.S., and Yang, Y.G. (2018). Dynamic transcriptomic m[6]A decoration: writers, erasers, readers and functions in RNA metabolism. Cell Res. *28*, 616–624.

Zhang, Y., Liu, T., Meyer, C.A., Eeckhoute, J., Johnson, D.S., Bernstein, B.E., Nusbaum, C., Myers, R.M., Brown, M., Li, W., and Liu, X.S. (2008). Model-based analysis of ChIP-seq (MACS). Genome Biol. *9*, R137.

Zheng, G., Dahl, J.A., Niu, Y., Fedorcsak, P., Huang, C.M., Li, C.J., Vågbø, C.B., Shi, Y., Wang, W.L., Song, S.H., et al. (2013). ALKBH5 is a mammalian RNA demethylase that impacts RNA metabolism and mouse fertility. Mol. Cell *49*, 18–29.

Zhou, C., Molinie, B., Daneshvar, K., Pondick, J.V., Wang, J., Van Wittenberghe, N., Xing, Y., Giallourakis, C.C., and Mullen, A.C. (2017). Genome-wide maps of m6A circRNAs identify widespread and cell-type-specific methylation patterns that are distinct from mRNAs. Cell Rep. *20*, 2262–2276.

STAR★METHODS

KEY RESOURCES TABLE

REAGENT or RESOURCE	SOURCE	IDENTIFIER
Antibodies		
Rabbit polyclonal anti-YTHDF2	Proteintech	Cat#24744-1-AP; RRID: AB_2687435
Rabbit polyclonal anti-HRSP12	Thermo Scientific	Cat#PA5-31352; RRID: AB_2548826
Rabbit polyclonal anti-POP1	Proteintech	Cat#12029-1-AP; RRID: AB_2166477
Rabbit polyclonal anti-RPP25	Proteintech	Cat#15461-1-AP
Mouse polyclonal anti-RPP20	ModiQuest	Cat#MQ 1.201-100
Rabbit polyclonal anti-METTL3	Proteintech	Cat#15073-1-AP; RRID: AB_2142033
Rabbit polyclonal anti-METTL14	Sigma-Aldrich	Cat#HPA038002; RRID: AB_10672401
Rabbit monoclonal anti-CNOT1	Proteintech	Cat#14276-1-AP; RRID: AB_10888627
Rabbit polyclonal anti-XRN1	Bethyl Laboratories	Cat#A300-443A; RRID: AB_2219047
Rabbit polyclonal anti-XRN2	Bethyl Laboratories	Cat#A301-103A; RRID: AB_2218876
Mouse monoclonal anti-snRNP70	Santa Cruz Biotechnology	Cat#sc-390899
Rabbit polyclonal anti-m^{6}A	Synaptic System	Cat#202 003; RRID: AB_2279214
Mouse monoclonal anti-β-actin	Sigma-Aldrich	Cat#A5441; RRID: AB_476744
Rabbit polyclonal anti-GAPDH	Ab frontier	Cat#LF-PA0212
Mouse monoclonal anti-FLAG	Sigma-Aldrich	Cat#A8592; RRID: AB_439702
Mouse monoclonal anti-FLAG	Sigma-Aldrich	Cat#A220
Mouse monoclonal anti MYC	Calbiochem	Cat#OP10L; RRID: AB_2266865
Rat monoclonal anti-HA	Roche	Cat#11 867 423 001
Rabbit polyclonal anti-GST	Bethyl Laboratories	Cat#A190-122A; RRID: AB_67419
Mouse monoclonal anti-His	GE Healthcare	Cat#27-4710-01; RRID: AB_771435
Bacterial and Virus Strains		
Escherichia coli Rosetta(DE3)pLysS	Novagen	Cat#70956
Escherichia coli BL21 (DE3)	Novagen	Cat#69450
Chemicals, Peptides, and Recombinant Proteins		
Cycloheximide	Sigma-Aldrich	Cat#01810
Dexamethasone (Dex)	Sigma-Aldrich	Cat#D4902
5,6-dichloro-1-β-D ribofuranosylbenzimidazole (DRB)	Sigma-Aldrich	Cat#D1916
GST	This paper	N/A
GST-human YTHDF2	This paper	N/A
GST-legionella RavZ	This paper	N/A
His-human HRSP12	This paper	N/A
Critical Commercial Assays		
Dynabeads Protein G for Immunoprecipitation	Invitrogen	Cat#10003D
Dynabeads Protein A for Immunoprecipitation	Invitrogen	Cat#10002D
SMARTer smRNA-Seq Kit for Illumina	Clontech	Cat#635031
Oligotex mRNA Midi Kit	QIAGEN	Cat#70042
NE-PER Nuclear and Cytoplasmic Extraction Reagents	Thermo Scientific	Cat#78835
Deposited Data		
mRNA-seq, CLIP-seq, and PARE-seq	This paper	SRP155278
Mendeley Data dataset	This paper	https://doi.org/10.17632/rxjghsgczt.1
Experimental Models: Cell Lines		
Human: HeLa	Korea Cell Line Bank	KCLB No. 10002; RRID: CVCL_0030
Human: HEK293T	ATCC	ATCC number: CRL-3216; RRID: CVCL_0063

Continued

REAGENT or RESOURCE	SOURCE	IDENTIFIER
Human: HRSP12 knock out HAP1	Horizon Discovery	Cat ID: HZGHC004874c001; RRID: CVCL_SR67
Human: Parental HAP1	Horizon Discovery	Cat ID: C631
Oligonucleotides		
siRNA sequences	See Table S6A	N/A
Oligonucleotides used for qRT-PCRs	See Table S6B	N/A
Biotinylated RNAs	See Table S6C	N/A
Recombinant DNA		
Plasmid: pMS2-HA	Cho et al., 2013	N/A
Plasmid: pMS2-HA-SMG5	Cho et al., 2013	N/A
Plasmid: pMS2-HA-PNRC2	Cho et al., 2013	N/A
Plasmid: pcβ-6bs	Cho et al., 2013	N/A
Plasmid: pcDNA3-FLAG-HRSP12-WT	Park et al., 2016	N/A
Plasmid: pcDNA3-FLAG-HRSP12-WT(P105A/R107E)	Park et al., 2016	N/A
Plasmid: pCMV-MYC-HRSP12	Park et al., 2016	N/A
Plasmid: pBG-SON-WT	Du et al., 2016	N/A
Plasmid: pBG-SON-Mut	Du et al., 2016	N/A
Plasmid: pBG-SON-WT-MT1	This paper	N/A
Plasmid: pBG-PLAC2-WT	Du et al., 2016	N/A
Plasmid: pBG-PLAC2-Mut	Du et al., 2016	N/A
Plasmid: pCMV-hPOP1-3xFLAG	Addgene	RRID: Addgene_53968
Plasmid: pGEx-4T-1-YTHDF1	Addgene	RRID: Addgene_70087
Plasmid: pcDNA3-FLAG-YTHDF2	Addgene	RRID: Addgene_52300
Plasmid: pGEx-4T-1-YTHDF3	Addgene	RRID: Addgene_70088
Plasmid: pCMV-MYC-YTHDF1	This paper	N/A
Plasmid: pCMV-MYC-YTHDF2	This paper	N/A
Plasmid: pCMV-MYC-YTHDF3	This paper	N/A
Plasmid: pcDNA3-FLAG-GFP	This paper	N/A
Plasmid: pMS-HA-YTHDF2	This paper	N/A
Plasmid: pMS2-HA-YTHDF2-N	This paper	N/A
Plasmid: pMS2-HA-YTHDF2-C	This paper	N/A
Plasmid: pMS2-HA-YTHDF2-1-100	This paper	N/A
Plasmid: pMS2-HA-YTHDF2-101-200	This paper	N/A
Plasmid: pMS2-HA-YTHDF2-201-383	This paper	N/A
Plasmid: pMS2-HA-YTHDF2(NΔ101-200)	This paper	N/A
Plasmid: pMS2-HA-GFP	This paper	N/A
Plasmid: pEBG-HRSP12	This paper	N/A
Plasmid: phCMV-MUP	Park et al., 2016	N/A
Plasmid: pcDNA3-FLAG	Park et al., 2016	N/A
Software and Algorithms		
riboPicker (v0.4.3)	Schmieder et al., 2012	http://ribopicker.sourceforge.net/
STAR aligner (v2.5.2b)	Dobin et al., 2013	https://github.com/alexdobin/STAR
HTseq (v0.6.1p1)	Anders et al., 2015	https://pypi.org/pypi/HTSeq
PARalyzer (v1.5)	Corcoran et al., 2011	https://ohlerlab.mdc-berlin.de/software/PARalyzer_85/
MACS (v1.4.2)	Zhang et al., 2008	http://liulab.dfci.harvard.edu/MACS/

CONTACT FOR REAGENT AND RESOURCE SHARING

Further information and requests for resources and reagents should be directed to and will be fulfilled by the Lead Contact, Yoon Ki Kim (yk-kim@korea.ac.kr).

EXPERIMENTAL MODEL AND SUBJECT DETAILS

HeLa and HEK293T cells were maintained in Dulbecco's modified Eagle's medium (Capricorn Scientific) supplemented with 10% (v/v) of fetal bovine serum (Capricorn Scientific) and 1% (v/v) of a penicillin/streptomycin solution (Capricorn Scientific). HAP1 cells were cultured in IMDM (GIBCO) containing 10% (v/v) of fetal bovine serum and 1% (v/v) of the penicillin/streptomycin solution. HRSP12-KO HAP1 cell lines were generated by means of a CRISPR-Cas9 system from Horizon Discovery. Where indicated, the cells were treated with 100 nM Dex (Sigma-Aldrich) for 1 h before cell harvesting.

METHOD DETAILS

Plasmid construction

The following constructs were described previously: pMS2-HA, pMS2-HA-SMG5, pcβ-6bs, and pMS2-HA-PNRC2 (Cho et al., 2013); pcDNA3-FLAG-HRSP12-WT, pcDNA3-FLAG-HRSP12-WT(P105A/R107E), and pCMV-MYC-HRSP12 (Park et al., 2016). pBG-SON-WT, pBG-SON-Mut, pBG-PLAC2-WT, and pBG-PLAC2-Mut were provided by Dr. Ligang Wu (Du et al., 2016). pCMV-hPOP1-3xFLAG (#53968), pGEx-4T-1-YTHDF1 (#70087), pcDNA3-FLAG-YTHDF2 (#52300), and pGEx-4T-1-YTHDF3 (#70088) were purchased from Addgene.

To construct pCMV-MYC-YTHDF1 and pCMV-MYC-YTHDF3, a XhoI/Klenow-filled EcoRI fragment of pGEx-4T-1-YTHDF1 containing YTHDF1 cDNA and XhoI/Klenow-filled BamHI fragment of pGEx-4T-1-YTHDF3 containing YTHDF3 cDNA were ligated to an XhoXI/Klenow-filled SalI fragment of pCMV-MYC (Clontech), respectively.

To generate pCMV-MYC-YTHDF2, an EcoRI/XhoI fragment of pCMV-MYC was ligated to two fragments: (i) a PCR-amplified EcoRI/NheI fragment containing YTHDF2 cDNA and (ii) a NheI/XhoI fragment of pcDNA3-FLAG-YTHDF2. The YTHDF2 cDNA was amplified by PCR from pcDNA3-FLAG-YTHDF2 as a template with specific oligonucleotides: 5′-CGGAATTCGCATGTCGGCCAGCAGCCTCTTGGAGC-3′ (sense) and 5′-TCAGTTTAGGTTGCTGTTTTGCAGG-3′ (antisense), where the underlined nucleotides specify the EcoRI site.

To construct pcDNA3-FLAG-GFP, a BamHI/HindIII fragment of pcDNA3-FLAG was ligated to a BamHI/HindIII fragment of GFP cDNA, which was amplified by PCR using pEGFP-C2 (Clontech) as a template and specific oligonucleotides: 5′-CGGGATCCGCTCGAGATGGTGAGCAAGGGCGAGGAGCTGTTC-3′ (sense) and 5′-CCCAAGCTTGCGGCCGCCTACTTGTACAGCTCGTCCATGCCGAGAGTG-3′ (antisense), where the underlined nucleotides specify the BamHI and HindIII sites, respectively.

For artificial tethering of YTHDF2 to the 3′ UTR of β-6bs mRNA, pMS-HA-YTHDF2, which expresses MS-HA-fused human full-length YTHDF2, was constructed by ligating a NotI/Klenow-filled EcoRI fragment of pCMV-MYC-YTHDF2 to a NotI/Klenow-filled XhoI fragment of pMS2-HA-PNRC2.

To construct pMS2-HA-YTHDF2-N and YTHDF2-C, a XhoI/NotI fragment of pMS2-HA-PNRC2 was ligated to a PCR-amplified XhoI/NotI fragment encoding an N- and C-terminal region of YTHDF2, respectively. The fragment encoding the N-terminal region of YTHDF2 was amplified by PCR using pcDNA3-MYC-YTHDF2 as a template and specific oligonucleotides: 5′-CCGCTCGAGATGTCGGCCAGCAGCCTCTTGGAGCAG-3′ (sense) and 5′-ATTTGCGGCCGCTCACAACACTGGGTGGGGTTCTGAAGG-3′ (antisense). The fragment encoding the C-terminal region of YTHDF2 was amplified by PCR using pcDNA3-MYC-YTHDF2 as a template and specific oligonucleotides: 5′-CCGCTCGAGGAGAAGCTTCGGTCCATAATAACTATAAC-3′ (sense) and 5′-ATTTGCGGCCGCTCATTTCCCACGACCTGACGTTCC-3′ (antisense), where the underlined nucleotides specify the XhoI and NotI sites.

To generate plasmids pMS2-HA-YTHDF2-1-100, YTHDF2-101-200, and YTHDF2 201-383, a PCR-amplified XhoI/NotI fragment coding for YTHDF2(1-100), YTHDF2(101-200), or YTHDF2(201-383) was ligated to a XhoI/NotI fragment of pMS2-HA-PNRC2, respectively. The fragments encoding YTHDF2(1-100), YTHDF2(101-200), and YTHDF2(201-383) were amplified by PCR using pcDNA3-MYC-YTHDF2 as a template and the following specific oligonucleotides: 5′-CCTCGAGATGTCGGCCAGCAGCCTCTTGGAGC-3′ (sense) and 5′-TTGCGGCCGCTCATAGGAAGTGGGGCTCTCCGTTGCTC-3′ (antisense) for the amplification of the fragment encoding YTHDF2(1-100); 5′-CCTCGAGCCAGATGCAATGTTTGGGCAACCAG-3′ (sense) and 5′-TTGCGGCCGCTCATGCAACTTCTGTGCTACCCAACTTC-3′ (antisense) for the amplification of the fragment coding for YTHDF2(101-200); and 5′-CCTCGAGAGCAATGTTCCAAAAGTTGTAG-3′ (sense) and 5′-TTGCGGCCGCTCATGAAGGAGTAGATCCAGAACCAGCC-3′ (antisense) for the amplification of the fragment encoding YTHDF2(201-383), respectively, where the underlined nucleotides specify the XhoI and NotI sites.

pMS2-HA-YTHDF2(NΔ101-200) was constructed by two-step PCR. First, the 5′ fragment encoding YTHDF2(1-100) and the 3′ fragment encoding YTHDF2(201-383) were amplified by means of PCR using pMS2-HA-YTHDF2-N as a template and specific oligonucleotides: (i) 5′-CTACCCATACGACGTTCCAGACTAC-3′ (sense) and 5′-GAACATTGCTTAGGAAGTGGGGCTCTCCGT-3′ (antisense) for the amplification of the 5′ fragment encoding YTHDF2(1-100) and (ii) 5′-CCACTTCCTAAGCAATGTTCCAAAAGTTGT-3′ (sense) and 5′-TCGAAGCATTAACCCTCACTAAAGG-3′ (antisense) for the 3′ fragment encoding YTHDF2(201-383).

Next, the two PCR-amplified fragments were mixed and reamplified via PCR with the sense oligonucleotide used for amplification of the 5′ fragment and the antisense oligonucleotide employed for amplification of the 3′ fragment. The resulting PCR-amplified fragment was digested with XhoI/NotI and then ligated to a XhoI/NotI fragment of pMS2-HA-YTHDF2-N.

To construct pMS2-HA-GFP, a PCR-amplified XhoI/NotI fragment containing GFP cDNA was ligated to a XhoI/NotI fragment of pMS2-HA-PNRC2. GFP cDNA was amplified by a PCR using pEGFP-C2 as a template and specific oligonucleotides 5′-CGGGATCCGCTCGAGATGGTGAGCAAGGGCGAGGAGCTGTTC-3′ (sense) and 5′-CCCAAGCTTGCGGCCGCCTACTTGTACA GCTCGTCCATGCCGAGAGTG-3′ (antisense), where the underlined nucleotides denote the XhoI and NotI sites, respectively.

pEBG-HRSP12 was generated by ligating a PCR-amplified BamHI/NotI fragment containing HRSP12 cDNA to BamHI/NotI-digested pEBG expressing GST. HRSP12 cDNA was amplified by PCR using pCMV-MYC-HRSP12 as a template and specific oligonucleotides: 5′-CGGGATCCATGTCGTCCTTGATCAGAAG-3′ (sense) and 5′-TTGCGGCCGCTTATAGTGATGCCGTTGTCA-3′ (antisense), where the underlined nucleotides specify the BamHI and NotI sites, respectively.

pBG-SON-WT-MT1 was constructed by two-step PCR. The 5′ fragment and the 3′ fragment were amplified by means of PCR using pBG-SON-WT as a template and specific oligonucleotides: (i) 5′-GGGCTGTTTTCATTTTCTCAGGCTG-3′ (sense) and 5′-CCCAAAGGA CTCGAAGTTGCTCTGGGTCCATGGTAAC-3′ (antisense) for amplification of the 5′ fragment and (ii) 5′-TGGACCCAGAGCAACTTCGAG TCTTTGGGGACCTG-3′ (sense) and 5′-GAACAATCAAGGGTCCCCAAACTCAC-3′ (antisense) for the 3′ fragment, where the underlined nucleotides specify the substitution sites. Next, the two PCR-amplified fragments were mixed and reamplified via PCR using the sense oligonucleotide used for amplification of the 5′ fragment and the antisense oligonucleotide used for amplification of the 3′ fragment. The resulting PCR-amplified fragment was digested with AccI/BamHI and then ligated to an AccI/BamHI fragment of pBG-SON-WT.

DNA or siRNA transfection

The cells were transiently transfected with the indicated plasmids using Lipofectamine 2000 (Invitrogen). Two days after transfection, the cells were harvested, and total protein and RNA were purified as described previously (Park et al., 2016).

To downregulate an endogenous protein, HeLa cells or HEK293T cells were transfected with 100 nM in vitro–synthesized siRNA (Gene Pharma) by means of Oligofectamine (Invitrogen). For a double knockdown, 200 nM siRNA was used in total. Three days after transfection, the cells were harvested, and total protein and RNA were purified as described previously (Park et al., 2016). The siRNAs used in our study are listed in Table S6A.

Protein expression and purification

Escherichia coli strain BL21(DE3) was transformed with a plasmid expressing GST, GST-YTHDF2, or GST-RavZ. Isopropyl β-D-thio-galactoside (1 mM) was added to the culture medium to induce the expression of GST-fused proteins, when absorbance at 600 nm reached 0.5. The cultures were then incubated for additional 16 h at 18°C. Recombinant His-HRSP12 was overexpressed in *E. coli* BL21(DE3) RIL by the addition of 1 mM isopropyl β-D-thio-galactoside, when absorbance at 600 nm was 0.5. After additional cultivation at 18°C for 16 h, the cells were harvested and resuspended in lysis buffer [50 mM Tris-HCl (pH 8.0), 200 mM NaCl, 1 mM Tris(2-carboxyethyl) phosphine, and 1 mM phenylmethanesulfonyl fluoride (PMSF)], and sonicated.

The GST-fused proteins were purified on a GST affinity column (GE Healthcare). His-HRSP12 and His-HRSP12(P105A/R107E) were purified on a Hi-trap nickel nitrilotriacetic acid column (GE Healthcare). Subsequent purification was conducted on a Hi-trap Q HP anion exchange column (GE Healthcare). Finally, all the recombinant proteins were subjected to gel filtration on a Hi-Load 16/600 Superdex 200 or 16/600 Superdex 75 column in a buffer [50 mM Tris-HCl (pH 7.5), 150 mM NaCl, and 1 mM Tris(2-carbox-yethyl) phosphine].

Antibodies

Primary antibodies against the following proteins were employed in this study [listed in the format "protein name (catalog number, supplier, fold dilution)"]: YTHDF2 (24744-1-AP, Proteintech, 1:1,000), HRSP12 (PA5-31352, Thermo Scientific, 1:1,000), POP1 (12029-1-AP, Proteintech, 1:1,000), RPP25 (15641-1-AP, Proteintech, 1:1,000), RPP20 (MQ 1.201-100, ModiQuest, 1:500), METTL3 (15073-1-AP, Proteintech, 1:1,000), METTL14 (HPA038002, Sigma, 1:250), CNOT1 (14276-1-AP, Proteintech, 1:1,000), XRN1 (A300-443A), XRN2 (A301-103A, Bethyl, 1:1,000), snRNP70 (sc-390899, Santa Cruz Biotechnology, 1:1,000), m^6A (202 003, Synaptic System, 1:50), β-actin (A5441, Sigma, 1:10,000), GAPDH (LF-PA0212, Ab Frontier, 1:10,000), FLAG M2 Peroxidase (A8592, Sigma, 1:5,000) for western blotting (WB), FLAG M2 Affinity Gel (A2220, Sigma) for IP, MYC (OP10L, Calbiochem, 1:1,000), HA (11 867 423 001, Roche, 1:10,000), GST (A190-122A, Bethyl, 1:8,000), and His (27-4710-01, GE Healthcare, 1:3,000).

Quantitative real-time RT-PCR

Total RNA was purified with the TRIzol Reagent (Life Technologies), and cDNA synthesis was carried out as described previously (Park et al., 2016). Quantitative real-time PCR analyses were performed with gene-specific primers and the Light Cycler 480 SYBR Green I Master Mix (Roche) on a Light Cycler 480 II machine (Roche). The oligonucleotides used in our study are listed in Table S6B.

Measurement of mRNA half-life

HeLa cells were transfected with siRNA or plasmids. Three or 2 days later, the cells were treated with 100 μg/mL 5,6-dichloro-1-β-D-ribofuranosylbenzimidazole (DRB; a potent transcription inhibitor; Sigma-Aldrich) at 6, 3, and 0 h before the cell harvesting (for

mRNA-seq experiments). For measuring the half-life of the reporter mRNAs, the cells were harvested at 0, 1, 2, and 3 h after DRB treatment. Total RNA was purified with the TRIzol Reagent (Life Technologies). For an mRNA-sequencing assay, ERCC RNA spike-in control (Ambion) was added to each sample according to the manufacturer's instructions before library construction. The half-life of transcripts was limited to 0–24 h.

Immunoprecipitation
IP procedures and RNA IP were performed on HeLa cells and HEK293T cells as described elsewhere (Park et al., 2016). Before the IPs, the extracts were treated with RNase A to prevent an RNA-mediated indirect interaction of proteins. A primary antibody against YTHDF2, HRSP12, POP1, m^{6}A, or FLAG was applied to IPs and RNA IPs.

In vitro GST pull-down assay
In these assays, purified recombinant GST, GST-YTHDF2, or GST-RavZ (25 μg) was mixed with His-HRSP12 (25 μg) and incubated in 200 μL of binding buffer [10 mM Tris-HCl (pH 8.0), 1% (v/v) glycerol, 150 mM NaCl, 0.1% Triton X-100, 2 mM benzamidine, 1 mM PMSF, and protease inhibitor mixture tablet (Roche)] at 4°C for 1 h. Glutathione Sepharose 4B resin (Amersham-Pharmacia Biotech) was added to the mixture and incubated at 4°C for 1 h. After quick centrifugation, the pellets were washed three times with binding buffer. The resin-bound proteins were resolved by SDS-PAGE and subjected to either Coomassie blue staining or WB.

In vitro CLIP using biotinylated RNAs
Biotin-labeled random 23-mer, GCAAC motif, and GGUUC motif RNAs were used for *in vitro* CLIP of HRSP12 (Figure 5J). Biotin-labeled random 41-mer, GCAAC-A motif, GCAAC-m^{6}A motif, GGUUC-A motif, and GGUUC-m^{6}A motif RNAs were employed for *in vitro* CLIP of HRSP12 and YTHDF2 (Figure 7E). All the biotin-labeled RNAs were purchased from GeneLink Inc. (Orlando, FL, USA). Sequence information on biotin RNAs is provided in Table S6C.

   In vitro CLIP involving biotinylated RNAs, which allows for measuring a direct protein-RNA interaction *in vitro*, was carried out as described elsewhere (Castello et al., 2012). For the preparation of cell extracts, HeLa cells were washed with ice-cold PBS and harvested by centrifugation at 3,000 × g for 10 min at 4°C. The cell pellets re-suspended with NET-2 buffer [50 mM Tris-HCl (pH 7.4), 150 mM NaCl, 1 mM PMSF, 2 mM benzamidine, and 0.05% NP-40] were sonicated on ice with 2 × 30 bursts of 1 s each (Branson Sonifier 250, output control 3, 30% duty cycle). After centrifugation at 13,000 × g for 10 min at 4°C, the supernatant was precleared by incubation with 50 μL of streptavidin resin (Thermo Scientific) for 1 h at 4°C. After preclearing and centrifugation at 13,000 × g for 1 min at 4°C, the supernatant was mixed with biotin-labeled RNAs (10 μg) in NET-2 buffer containing 100 U of an RNase inhibitor (Thermo Scientific) at 30°C for 30 min and irradiated with ultraviolet (UV; 254 nm, 500 mJ/cm^2) light using a UV cross-linker (UVP). Then, 50 μL of streptavidin agarose resin was mixed with each cell extract and incubated at 4°C for 3 h. After that, the biotinylated RNA-bound resin samples were washed with a buffer containing decreasing concentration of LiCl and LiDS. In brief, the biotinylated RNA-bound resin samples were washed with the following buffers, in this order: buffer 1 [20 mM Tris-HCl (pH 7.5), 500 mM LiCl, 1 mM EDTA, 5 mM DTT, and 0.5% LiDS], buffer 2 [20 mM Tris-HCl (pH 7.5), 500 mM LiCl, 1 mM EDTA, 5 mM DTT, and 0.1% LiDS], buffer 3 [20 mM Tris-HCl (pH 7.5), 500 mM LiCl, 1 mM EDTA, 5 mM DTT, and 0.01% NP-40], and buffer 4 [20 mM Tris-HCl (pH 7.5), 200 mM LiCl, 1 mM EDTA, and 5 mM DTT]. The resin-bound proteins were eluted with LiDS sample buffer (Invitrogen) and subjected to western blotting.

In vivo CLIP
In vivo CLIP experiments were carried out as CLIP-seq with slight modifications. In brief, HeLa cells were irradiated with UV light (254 nm, 400 mJ/cm^2) using a UV cross-linker (UVP) before harvesting. The cross-linked cell pellets were resuspended with 600 μL of lysis buffer [20.3 mM Na$_2$HPO$_4$, 3.5 mM KH$_2$PO$_4$, 6.8 mM KCl, 342.5 mM NaCl, 0.1% SDS, 0.5% sodium deoxycholate, and 0.5% NP-40 (pH 7.2)] and incubated for 10 min on ice. RNase-free DNase I (30 U; Thermo Scientific) was added to the cell lysates. After centrifugation at 13,000 × g for 20 min at 4°C, the supernatants were mixed with protein A Dynabeads (Invitrogen) preincubated with the primary antibody for 2 h at 4°C and subjected to IP. The beads were washed twice with lysis buffer and with PNK buffer [50 mM Tris-HCl (pH 7.4), 10 mM MgCl$_2$, and 0.5% NP-40]. The resin-bound protein and RNA were purified as described previously (Park et al., 2016).

In vitro RNA cleavage assay
RNA substrates were synthesized by *in vitro* transcription of a XhoI fragment of pSK-C5′ (Park et al., 2016) as a template, T7 RNA polymerase (New England Biolabs), 10 mM NTPs, and 250 μCi [α-^{32}P]UTP. *In vitro*–transcribed RNAs were incubated with 100 ng of purified recombinant His-HRSP12, His-HRSP12(P105A/R107E), or RNase A, as a positive control, in reaction buffer [10 mM Tris-HCl (pH 7.4), 100 mM NaCl, and 2 mM MgCl$_2$] at 37°C for 1 h. After that, the purified RNAs were analyzed on 10% urea gels and subjected to autoradiography with FLA7000 (Fuji Photo Film Co.).

Far-western blotting
Far-western blotting was performed using purified recombinant GST, GST-YTHDF2, GST-RavZ, and His-HRSP12. Briefly, the purified recombinant proteins were resolved by SDS-PAGE and transferred to a Hybond ECL nitrocellulose membrane (Amersham

Biosciences). The membrane was incubated for 24 h at 4°C in blocking buffer [100 mM Tris (pH 7.4), 100 mM potassium acetate, 2 mM magnesium acetate, 0.1 mM EDTA, 10% glycerol, 1 mM PMSF, 1 mM benzamidine, and 0.05% Tween 20] containing 5% of skimmed milk. The membrane was next incubated for 24 h at 4°C in blocking buffer containing immunopurified POP1-FLAG or FLAG-GFP. Then, the membrane was washed once with blocking buffer and twice with TBS [25 mM Tris (pH 7.4), 150 mM NaCl, 2 mM KCl, and 0.05% Tween 20]. The washed membrane was analyzed by WB with an α-FLAG antibody.

Nucleocytoplasmic fractionation

These procedures were performed according to manufacturer's instructions for NE-PER Nuclear and Cytoplasmic Extraction Reagents (Thermo Scientific).

mRNA sequencing

HeLa cells were transiently transfected with control siRNA or siRNA against *YTHDF2*, *HRSP12*, *POP1*, *RPP20*, or *CNOT1*. Three days later, total-cell RNA was purified using TRIzol and subjected to library construction procedures and mRNA sequencing assays, which were performed by Macrogen Inc. In brief, the RNA integrity number was measured on a bioanalyzer (Agilent). The purified RNA samples were next subjected to mRNA-seq library construction using the TruSeq Stranded mRNA Sample Preparation Kit (Illumina). The constructed cDNA libraries were validated regarding size distribution on an Agilent Bioanalyzer (DNA 1000 kit; Agilent), quantitated by qPCR (Kapa Library Quant Kit; Kapa Biosystems, Wilmington, MA), and then adjusted to 2 nmol/L for NGS on the Illumina HiSeq 2500 platform (100-base paired-end reads). The Pearson correlation coefficients (*r*) of two biological replicates of mRNA-seq using total-cell RNAs of the cells either undepleted or depleted of each factor were greater than 0.945, indicating a strong correlation between the two replicates (Table S1).

CLIP sequencing (CLIP-seq)

CLIP-seq experiments were carried out as previously described (Murigneux et al., 2013; Ryu et al., 2019) with slight modifications. In brief, HeLa cells were irradiated with ultraviolet (UV; 254 nm, 400 mJ/cm^2) light using a UV cross-linker (UVP) before harvesting. The cross-linked cell pellets were mixed with 600 μL of lysis buffer [20.3 mM Na$_2$HPO$_4$, 3.5 mM KH$_2$PO$_4$, 6.8 mM KCl, 342.5 mM NaCl, 0.1% SDS, 0.5% sodium deoxycholate, and 0.5% NP-40 (pH 7.2)] and incubated for 10 min on ice. RNase-free DNase I (30 U; Thermo Scientific) was added to the cell lysates and incubated at 37°C for 5 min. Then, 0.1 or 1 ng of RNase A (Affymetrix) was additionally introduced with incubation for 10 min at 37°C. After centrifugation at 13,000 × *g* for 20 min at 4°C, the supernatants were subjected to IP with protein G Dynabeads (Invitrogen) preincubated with the primary antibody for 2 h at 4°C. The beads were washed twice with lysis buffer and with PNK buffer [50 mM Tris-HCl (pH 7.4), 10 mM MgCl$_2$, and 0.5% NP-40].

To eliminate the terminal phosphates, the beads were mixed with 40 U/mL alkaline phosphatase (Roche) and incubated for 10 min at 37°C. The beads were then washed twice with PNK+EGTA buffer [50 mM Tris-HCl (pH 7.4), 0.5% NP-40, and 20 mM EGTA] and twice with PNK buffer. To phosphorylate the 5′ end of RNAs, the beads were mixed with 0.5 U/μl T4 polynucleotide kinase (T4 PNK; New England Biolabs) and 0.125 mM ATP in PNK buffer for 10 min incubation at 37°C. The beads were then washed twice with PNK+EGTA buffer. Finally, RNAs and proteins bound to the beads were eluted by means of lithium dodecyl sulfate sample buffer (Invitrogen).

To isolate RNA covalently cross-linked to proteins, the samples were separated by SDS-PAGE in a Novex NuPAGE Bis-Tris gel (Invitrogen) and transferred to a nitrocellulose membrane. A piece of the membranes ranging from the molecular weight of the immunoprecipitated protein to approximately 20 kDa above was excised. The piece of membrane was soaked in PK buffer [100 mM Tris-HCl (pH 7.4), 50 mM NaCl, and 10 mM EDTA] containing 4 mg/mL proteinase K (Roche), incubated for 20 min at 37°C, and next incubated in PK/Urea buffer [100 mM Tris-HCl (pH 7.4), 50 mM NaCl, 10 mM EDTA, and 7 M urea] for 20 min at 37°C. The supernatants were subjected to organic extraction and ethanol precipitation with GlycoBlue (Ambion) to precipitate RNA fragments.

Construction of small RNA libraries was performed by means of the SMARTer® smRNA-Seq Kit for Illumina® (Clontech). Sequencing was carried out using an Illumina HiSeq 2500 system (Illumina). Sequencing was carried out in single-end mode (1 × 100 bp) on an Illumina HiSeq 2500 system (Illumina, CA, USA). The sequencing was conducted by Macrogen Inc.

PARE sequencing (PARE-seq)

PARE-seq experiments were conducted as previously described (German et al., 2008; Schmidt et al., 2015) with some modifications. In brief, HeLa cells were transfected with XRN1/2 siRNA and siRNA against *YTHDF2*, *HRSP12*, or *POP1*. Three days later, total-cell RNAs were purified with the TRIzol Reagent. Polyadenylated RNAs were purified using the Oligotex mRNA kit (QIAGEN). The purified RNAs were ligated to an RNA oligonucleotide adaptor (5′-GUUCAGAGUUCUACAGUCCGAC-3′) using T4 RNA ligase (New England Biolabs), where the underlined nucleotides specify an MmeI site. The ligated products were purified with the Oligotex mRNA kit again and were used as a template in a reverse-transcription reaction with the oligonucleotide 5′-CGAGCACAGAATTAATACGACT(18)V-3′ and reverse transcriptase (Thermo Scientific) for the first-strand cDNA synthesis. Then, the cDNA was amplified with DNA polymerase (Solgent) and specific oligonucleotides: 5′-GTTCAGAGTTCTACAGTCCGAC-3′ (sense) and 5′-CGAGCACA GAATTAATACGACT-3′ (antisense). The PCR conditions were as follows: 7 cycles of 94°C for 20 s, 68°C for 30 s, and 72°C for 3 min. The PCR products were cleaved with MmeI (New England Biolabs), and the cleavage products corresponding to ~42 nucleotides in length were excised from the gel. The products were ligated to a double-stranded DNA adaptor with a 2-nucleotide

degenerate 3′ overhang (top strand: 5′-P-TGGAATTCTCGGGTGCCAAGG-3′; bottom strand 5′- CCTTGGCACCCGAGAATTC CANN-3′; P specifies a phosphate group) using T4 DNA ligase (Roche). The ligated products (63 nucleotides long) were then isolated by gel purification and amplified by PCR with the following oligonucleotides: [P5 primer (5′-AATGATACGGCGACCACCGACAGGTT CAGAGTTCTACAGTCCGA-3′) and P7 index primer (5′-CAAGCAGAAGACGGCATACGAGATXXXXXXGTGACTGGAGTTCCTTGG CACCCGAGAATTCCA-3′; the XXXXXX site indicates a 6-nucleotide index sequence)]. The PCR products (126 nucleotides in length) were purified and subjected to NGS on the HiSeq 2500 platform (Illumina) by Macrogen Inc.

General processing and mapping of reads
NGS raw data were preprocessed in the following order: trimming of adaptor and poly(A) sequences by means of Cutadapt (https:// cutadapt.readthedocs.io/en/stable/#), filtering out ribosomal sequences in the riboPicker software (Schmieder et al., 2012) with a customized rRNA dataset. At the adaptor-trimming step, the read lengths over 15 bp and with Phred quality score $\geq$ 30 were filtered for further analysis. For PARE-seq analysis, only the reads ranging from 20 to 21 nucleotides were selected. The filtered reads were aligned to the reference human genome (hg19) via the STAR software (Dobin et al., 2013). Only uniquely mapped reads were chosen for subsequent analyses. The correlations between two independent biological replicates in each experiment were determined by means of the NumPy library in Python.

The numbers of reads obtained from stepwise processing are summarized in Tables S1–S3 (Table S1 for mRNA-seq; Table S2 for HRSP12 CLIP-seq; and Table S3 for PARE-seq).

Transcriptome analysis and RNA half-life profiling
The mapped reads from mRNA sequencing were quantified in FPKM via Cufflinks version 2.2.1 (http://cole-trapnell-lab.github.io/ cufflinks/). Differentially expressed genes (DEGs) were found by means of the Cuffdiff program, a part of the Cufflinks software package.

For GO analysis, the 328 gene symbols of interest (H∩Y∩P) were uploaded to DAVID (https://david.ncifcrf.gov/) and then analyzed with the functional annotation tool. The identified GO terms and their corresponding P values were retrieved from the downloaded output files: molecular function (level 4) and biological process (level 3) terms (Table S4).

RNA half-life data were analyzed by removal of unwanted variation-based normalized read counts. A customized reference sequence, which was defined as the union of the human reference genome (hg19) and the 92 ERCC spike-in control sequences, was used for mapping. The read counts per gene were estimated using the htseq-count Python code (Anders et al., 2015). With the normalized read counts, the half-life of a transcript was calculated according to a known formula (Wang et al., 2014).

CLIP peak calling and analysis
The peak calling of HRSP12 CLIP was conducted in the piranha software (http://smithlabresearch.org/software/piranha/) with specific option settings (-b 20 -a 0.9) with covariates (mRNA-seq of input). The YTHDF2 peaks were obtained by PARalyzer ver. 1.5 (Corcoran et al., 2011), an algorithm measuring T-to-C conversions, with default settings from published PAR-CLIP data (Wang et al., 2014).

Annotation of the exonic regions of mRNAs and noncoding RNAs was retrieved from two publicly available databases: RefSeq Genes [hg19; UCSC table browser (http://genome.ucsc.edu/cgi-bin/hgTables)] and GENCODE (Release 19). To obtain the intronic region of those RNAs, the subtractBed module from Bedtools v.2.25.0 was employed (https://bedtools.readthedocs.io/en/stable/#). Six hierarchical categories were set up according to the following annotation: CDSs > 5′ UTRs > 3′ UTRs > lncRNAs > introns of mRNAs > intron of lncRNAs. Then, the called CLIP peaks were assigned to each genomic region category using the intersectBed function from Bedtools. To measure the relative peak distribution in each category, the number of peaks was normalized to the length of the corresponding region.

Metagene analysis
Only the longest mRNA among alternative isoforms (RefSeq genes) was considered a representative in the metagene analysis. The centers of all CLIP peaks obtained from two biological replicates of CLIP-seq experiments were displayed on their corresponding regions: 5′ UTR, CDS, and 3′ UTR. Each region was binned into 50 segments and smoothed by the nearest-neighbor method (k = 3). Only two (SRR944646 and SRR944648) out of three replicates from published YTHDF2 CLIP data (Wang et al., 2014) were used to obtain peaks, because the data size of the rest was too small to compare with others.

Consensus motif analysis
The consensus motif from HRSP12 CLIP peaks was identified with the HOMER package (v.4.8.3) and MEME (v.5.0.1). The motif length was restricted to 10 nucleotides in HOMER or 5-10 nucleotides in MEME. Then, the predicted motif with the lowest P values or E value was selected.

m⁶A-seq analysis
m⁶A-containing genes were analyzed on the basis of previously published data (Wang et al., 2014). Peaks were obtained in the model-based analysis of ChIP-seq (MACS) peak-calling software with m⁶A input as control, as previously described (Zhang et al.,

2008). The relative distance from HRSP12 CLIP peaks was calculated by the method that was used to measure the distance between MaxPeak and MaxSeq (refer to the "Relative distances between CLIP MaxPeaks and PARE MaxSeqs" subsection).

PARE analysis

The PARE analysis was carried out as previously described (Schmidt et al., 2015) with slight modifications. The 5′ end of the PARE mapped reads was defined as a PARE sequence. The functional PARE sequences were selected as follows (Table S3): abundance of the genes containing a PARE sequence: FPKM ≥ 5; tags per 5 million (TP5M) ≥ 100 in the cells treated with siXRN1/2; and the ratio of TP5M in the cells treated with siXRN1/2 to that in the cells simultaneously treated with siXRN1/2 and other siRNA ≥ 2. The most abundant PARE sequence in an individual gene was identified and defined as PARE MaxSeq. Nucleotide composition analysis of the 10-nucleotide regions surrounding 2,257 PARE MaxSeqs was carried out by in-house python code.

CDF analysis

To compare the cumulative distribution of transcript input before and after downregulation of YTHDF2, HRSP12, POP1, RPP20, or CNOT1 (Figure 4), four groups (non-targets, CLIP–IP, CLIP, and CLIP∩IP targets) categorized in a previous study (Wang et al., 2014) were used. In particular, only the genes with FPKM ≥ 5 in our mRNA-seq of siControl-treated cells were considered for the CDF analysis in this study.

In case of HRSP12 CLIP targets (Figure 5B), we obtained peak-containing common genes from two biological replicates of HRSP12 CLIP-seq experiments. The common genes (in the overlap) between the gene set of HRSP12 CLIP targets and the previously categorized gene set of YTHDF2 CLIP targets were categorized as H∩Y transcripts (Figures 5C–5G).

To compute the $\log_2$ ratio of siYTHDF2 to siControl, the Cuffdiff output of mRNA-seq data was used. The genes with FPKM = 0 in our mRNA-seq were ignored. The CDF plots were generated by an in-house Python script. P values between targets and non-targets were calculated by two-tailed Mann–Whitney U test. Previously reported mRNA-seq data (sequenced by NextSeq 500) from HRSP12-depleted HeLa cells (Park et al., 2016) and total RNA-seq data from *RMRP* knockdown HeLa cells (Goldfarb and Cech, 2017) were also analyzed via the same strategy.

Relative distances between CLIP MaxPeaks and PARE MaxSeqs

For the simple comparison of the distance, we first determined a MaxPeak, which was defined in our study as the most abundant CLIP peak in exons of an individual gene. After that, the distances between MaxSeq and MaxPeak in individual protein-coding genes and mRNAs were analyzed. Among isoforms of the same gene, the minimal distance was chosen. P values between MaxSeq and MaxPeak were calculated by the one-tailed Mann–Whitney U test. The genomic positions of YTHDF2 MaxPeak, HRSP12 MaxPeak, and PARE MaxSeq among the 115 mRNAs targeted by the YTHDF2-HRSP12-RNase P/MRP pathway are listed in Table S5.

mRNA length distribution

To characterize the length distribution of mRNAs within the H∩Y∩P group, only the longest mRNA among alternative isoforms (RefSeq genes) was chosen. The Kolmogorov–Smirnov test performed in the scipy.stats.ks_2samp module of the SciPy Python library was applied to the statistical test of the difference in the length between total mRNAs and mRNAs in the H∩Y∩P group.

QUANTIFICATION AND STATISTICAL ANALYSIS

Two-tailed and equal-variance Student's t test was performed for statistical analysis with significance defined as a P value < 0.05 or < 0.01. In most cases, data obtained from at least three independently performed biological replicates were analyzed, unless indicated otherwise in the Figure legends section. Data are presented as the mean ± standard deviation.

For Figure 1D, the levels of coIPed proteins were normalized to the amount of IPed YTHDF2. Then, the normalized levels obtained in the immunoprecipitates of YTHDF2 in undepleted cells were arbitrarily set to 1.0. Downregulation efficiency was also calculated by comparing the levels of proteins between undepleted and HRSP12-depleted cells.

In case of CDF analysis, P values were calculated by the two-tailed Mann–Whitney U test. For measuring the distance between MaxSeq and MaxPeak and for the CDF analysis of double knockdown samples, P values were calculated by the one-tailed Mann–Whitney U test. For the analysis of correlation between mRNA sequencing data obtained from two biological replicates, Pearson's correlation coefficients (r) were calculated. In case of analysis of gene length distribution, the Kolmogorov–Smirnov test was applied.

DATA AND SOFTWARE AVAILABILITY

The accession number for the next-generation sequencing data reported in this paper is NCBI Sequence Read Archive: SRP155278. Raw data images can be found at https://doi.org/10.17632/rxjghsgczt.1.